Using Cerebral Organoids to Model HCMV Infection in the Developing Brain

A Thesis

Presented in Partial Fulfillment of the Requirements

for the Degree of Master of Science

with a

Major in Microbiology, Molecular Biology and Biochemistry

in the

College of Graduate Studies

University of Idaho

by

Rebecca McKenzie Brown

Major Professor: Elizabeth A. Fortunato, Ph.D.

Committee Members: Tanya Miura, Ph.D.; Peter Fuerst, Ph.D.; Anthony Nicola, Ph.D.

Department Administrator: James Nagler, Ph.D.

June 2016

AUTHORIZATION TO SUBMIT THESIS

This thesis of Rebecca McKenzie Brown, submitted for the degree of Master of Science with a Major in Microbiology, Molecular Biology and Biochemistry and titled "Using Cerebral Organoids to Model HCMV Infection in the Developing Brain," has been reviewed in final form. Permission, as indicated by the signatures and dates below, is now granted to submit final copies to the College of Graduate Studies for approval.

Major Professor: _____ Date: _____
Elizabeth A. Fortunato, Ph.D.

Committee Members: _____ Date: _____
Tanya Miura, Ph.D.

_____ Date: _____
Peter Fuerst, Ph.D.

_____ Date: _____
Anthony Nicola, Ph.D.

Department Administrator: _____ Date: _____
James Nagler, Ph.D.

ABSTRACT

Human cytomegalovirus (HCMV) is a leading cause of congenital birth defects in the United States. It causes neurological deficits such as deafness, blindness, microcephaly, mental retardation, and cerebral calcification, among others (Cannon 2009). These birth defects are well characterized, but little is known about the mechanisms underlying them. In the present study, we mapped DNA breaks at 1q42, investigated potential sequence changes by incorrect repair, and sought to predict how a viral protein may be interacting with the break sites. To understand how HCMV infection impacts the brain of a developing fetus, we used cerebral organoids. Uninfected organoids were characterized by the morphology and protein expression of their internal structures. We determined that organoids could be infected with HCMV and found abnormal beta tubulin III staining in areas of viral antigen positivity, as well as a decrease in nidogen-1 expression.

ACKNOWLEDGEMENTS

I would like to thank my major professor Dr. Elizabeth Fortunato for giving me the opportunity to work on a project that I love and for providing her guidance and support throughout the last two years.

Thank you to John O'Dowd, Man I Kuan, and Aaron Simmons for their help in the lab and for their friendship.

Additionally, I would like to thank all my committee members for their support and advice throughout my undergraduate and graduate careers.

DEDICATION

Thank you to my parents, Mark and Tana McKenzie, for everything that you have done for me throughout my academic career. Without their support and words of wisdom, I would not have been able make it through the last two years.

I want to give a very special thanks to Vern and Barbara Cromwell who, without realizing it, nurtured my love of science and continue to inspire me. Even though they are not around to see the completion of this thesis, they were instrumental in my decision to continue on to graduate school.

Thank you to my friends Kelley Verner, Kyle Richards, Jacob Westacott, Ingrid Kooda, Cody Steven, and Mike Affeldt for the overwhelming amount of emotional support. You guys rock.

Finally, I want to thank my wonderful husband, Micah Brown, for pushing me when I felt like quitting. He helps me to be a better person and scientist.

TABLE OF CONTENTS

LIST OF FIGURES

LIST OF TABLES

CHAPTER 1: LITERATURE REVIEW

Literature Review

HCMV Clinical Significance

Human cytomegalovirus (HCMV) is a beta-herpesvirus that infects 60-70% of adults in industrialized countries (Staras et al. 2006). Healthy adults are usually asymptomatic. For those that are immune-compromised, such as organ transplant recipients and AIDS patients, it can cause kidney, liver and CNS damage (Reuter et al. 2004). HCMV is also a leading cause of birth defects in the United States, affecting an estimated 8,000 children per year. More children are affected by HCMV-related defects than fetal alcohol syndrome or Down syndrome (Cannon and Davis 2005). Infected children can develop serious neurological symptoms, such as blindness, deafness, cerebral calcification, and microcephaly, among others. 1% of newborns are congenitally infected with the virus every year (Cannon 2009). 5-10% of infected newborns will show neurological defects at birth, while another 10-15% will develop them later in childhood (Dollard et al. 2007). Like other herpesviruses, HCMV can establish a lifelong latent infection. Transmission to the fetus can occur from a reactivation event as well as primary infection during pregnancy (Boppana et al. 2001). Fetuses infected with HCMV during the first trimester of gestation are more likely to have neurological defects, especially sensorineural hearing loss (Pass et al. 2005). Although the negative consequences of congenital HCMV infection are well documented, the mechanisms underlying them are not clear.

Morphology and Replication Cycle

HCMV is a double stranded DNA virus that has the largest genome of all the herpesviruses. The 235 kbp viral genome encodes over 200 open reading frames (ORFs) and is enclosed in an icosahedral protein capsid that protects the genome as it traffics towards the nucleus (Varnum et al. 2004). Tegument proteins and a lipid envelope enclose the capsid (figure 1). The tegument proteins lie between the envelope and the capsid, provide protection for the capsid, and can transactivate the expression of viral genes during infection. The envelope carries virus-encoded glycoproteins that mediate fusion with the plasma membrane of the host cell.

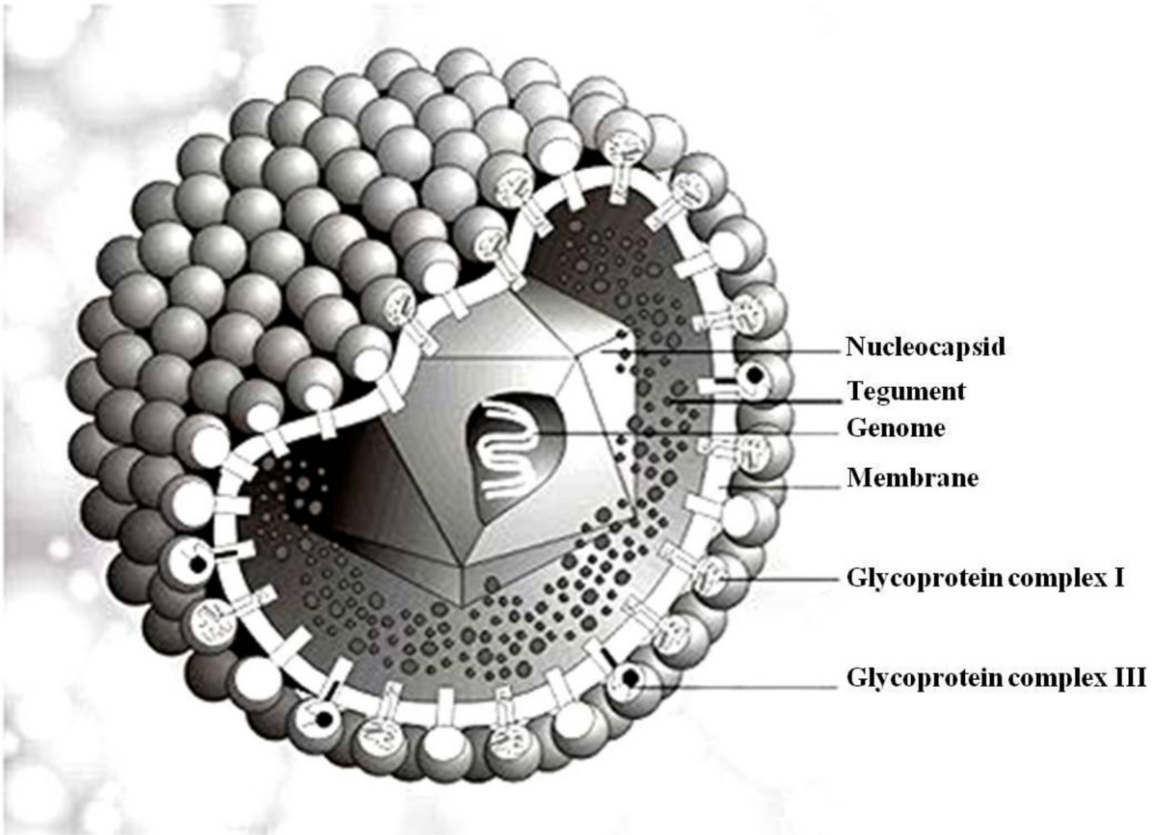

Figure 1: The structure of the HCMV virion includes the genome, protein capsid, tegument proteins, lipid envelope, and surface glycoproteins. Photo courtesy of Marko Reschke in Marburg, Germany.

Glycoprotein B (gB) is the most highly conserved glycoprotein on the lipid envelope and is responsible for binding and entry into host cells, cell-to-cell transmission, and fusion of adjacent cells (Varnum et al. 2004). gB binds to the heparin sulfate proteoglycan receptor for viral entry and is expressed on the membranes of infected cells during late stages of infection (Varnum et al. 2004). The glycoproteins gH and gL also participate in membrane fusion by forming a complex with other proteins. They can bind to gO, another glycoptotein, to form the gH/gL/gO complex. gH and gL can also bind proteins UL128, UL130, and UL131 to form the gH/gL/UL128-131 complex. Recent work suggests that these protein complexes are responsible for cell tropism. Strains that lack UL128-131 replicate well in fibroblasts, but not in epithelial or endothelial cells (Ryckman et al. 2007). The latest research suggests that the abundance of gH/gL and gH/gL/UL128-131 on the surface of the virion may dictate its ability to enter different cell types (Zhou et al. 2015).

Interaction of the viral envelope and its glycoproteins with the cell membrane causes the membranes to fuse, delivering the capsid and tegument proteins into the cytoplasm (Tomtishen III 2012). The capsids then traffic to the nucleus and deposit the viral genome. Select tegument proteins, such as pp65 and pp71, traffic to the nucleus independently of the capsids. After the viral genome enters the nucleus, viral immediate early genes are expressed in a lytic infection. During latent infection, immediate early gene expression is repressed due to an inability of pp71 to transit to the nucleus and counteract the cells anti-viral response and no new viruses are produced (Kalejta 2008).

There are three different classes of viral genes, immediate early (IE), early (E), and late (L) that are expressed during lytic infection. The major immediate early promoter (MIEP) controls the expression of IE genes. IE gene expression is modulated by the interaction of the cellular protein DAXX and viral tegument protein pp71 at the MIEP (Woodhall et al. 2006 and Lukashchuk et al. 2008). Tegument protein pp71 transactivates the MIEP and IE genes are expressed. DAXX is a transcriptional repressor that can silence IE gene expression via histone de-acetylase (HDAC) (Lukashchuk et al. 2008). The expression of IE genes activates expression of E genes, which generally encode viral proteins important for viral DNA replication, such as DNA polymerase. Late viral proteins encode structural elements that allow the assembly of the new viral progeny. During latent infection, there is no IE gene transcription and no new virions are produced. The MIEP is repressed via histone methylation and de-acetylation and DAXX activity suppresses lytic transcription (Lukashchuk et al. 2008). In un-differentiated cell types, such as embryonic stem cells (ESCs), pp71 is localized to the cytoplasm and viral genomes co-localize with DAXX and HDACs, among others at the nuclear-domain 10 (ND10) bodies. This causes the viral genome to be heterochromatinized, and IE gene expression is subsequently repressed. In terminally differentiated cell types, such as fibroblasts, lytic infection is initiated upon infection with HCMV. During infection of these cells, pp71 localizes to the nucleus and prevents DAXX from silencing the viral genome (Penkert and Kalejta 2013).

Once viral DNA is replicated and late structural proteins are expressed, DNA is packaged into capsids (Britt 2007). The capsids acquire a primary envelope by budding through the inner nuclear membrane and into the perinuclear space. Subsequent

budding through the outer nuclear membrane and into the cytoplasm removes the primary envelope (Britt 2007). The capsid acquires the majority of tegument proteins in the cytoplasm and acquires its final envelope by budding through Golgi derived vesicles. Fusion of these vesicles with the outer cell membrane releases the enveloped virion (Sinclair 2006).

HCMV Induced Breaks on Chromosome One

Previous work has shown that HCMV causes breaks at two distinct locations on chromosome one, 1q42 and 1q23 (Fortunato et al. 2000). Breaks can occur at each site alone or at both simultaneously (Figure 2A) and occur as early as 15 minutes post infection (pi) (Figure 2B). At 24 hours post infection (hpi), 30% of infected fibroblasts are broken at the 1q42 locus, declining to 15% over 120 h. A decline in the frequency of breaks over 120 h suggests the DNA is being repaired. UV inactivated (transcriptionally inactive) virus also breaks the DNA, meaning the viral candidate protein contributing to DNA damage is not *de novo* synthesized, but rather is brought in with the virus. Previous work has shown that HCMV inhibits the host cell's DNA damage response (DDR), leaving chromosomal breaks incompletely repaired without arrest or apoptosis. Additionally, the HCMV genome is preferentially repaired over the host genome during infection (O'Dowd et al. 2012). Improper DNA repair at these break sites could introduce mutations, which are detrimental to the development of the fetus and can potentially lead to the down-regulated expression of break-site encoded genes. Although the breaks have been broadly mapped and characterized, finer mapping using

ligation mediated PCR (LM-PCR) is needed to pinpoint their locations. This work will be described in greater detail in chapter two.

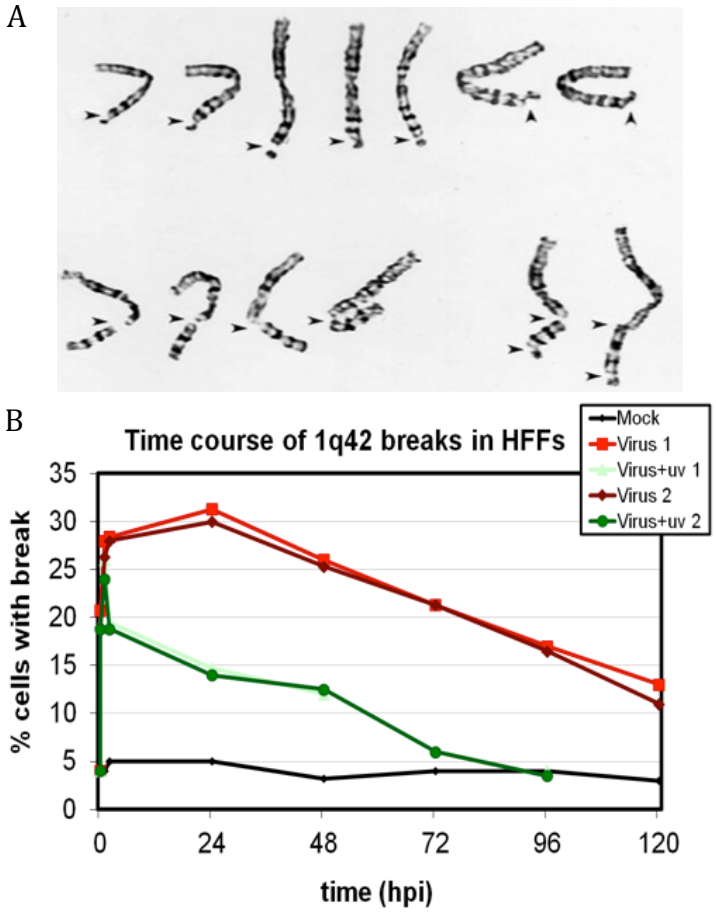

Figure 2: (A) Giemsa banding shows several different examples of the types of breaks observed at chromosome one. They can occur at position 1q42 only (upper), at position 1q23 only (lower left), or a double break at both positions (lower right) (Fortunato et al. 2000). (B) FISH analysis using human foreskin fibroblasts (HFFs) shows break frequency at 1q42 is maximal at 24 hpi and declines over 120 h. Cells infected with UV irradiated virus initially have the same percentage of breaks, but decline to the level of mock-infected cells by 96 h (work of Deborah Duricka).

The locus surrounding the 1q42 break site contains the gene nidogen 1 (NID1), CCCTC-binding factor (CTCF) binding sites, and DNAse hypersensitivity sites (Figure 3). The 1q23 locus is strikingly similar to the 1q42 site, with CTCF binding sites, DNAse hypersensitivity sites, and an adjacent gene, myelin protein zero (MPZ). The structural

similarity of both of these sites suggests the breaks could be caused by similar viral protein interaction.

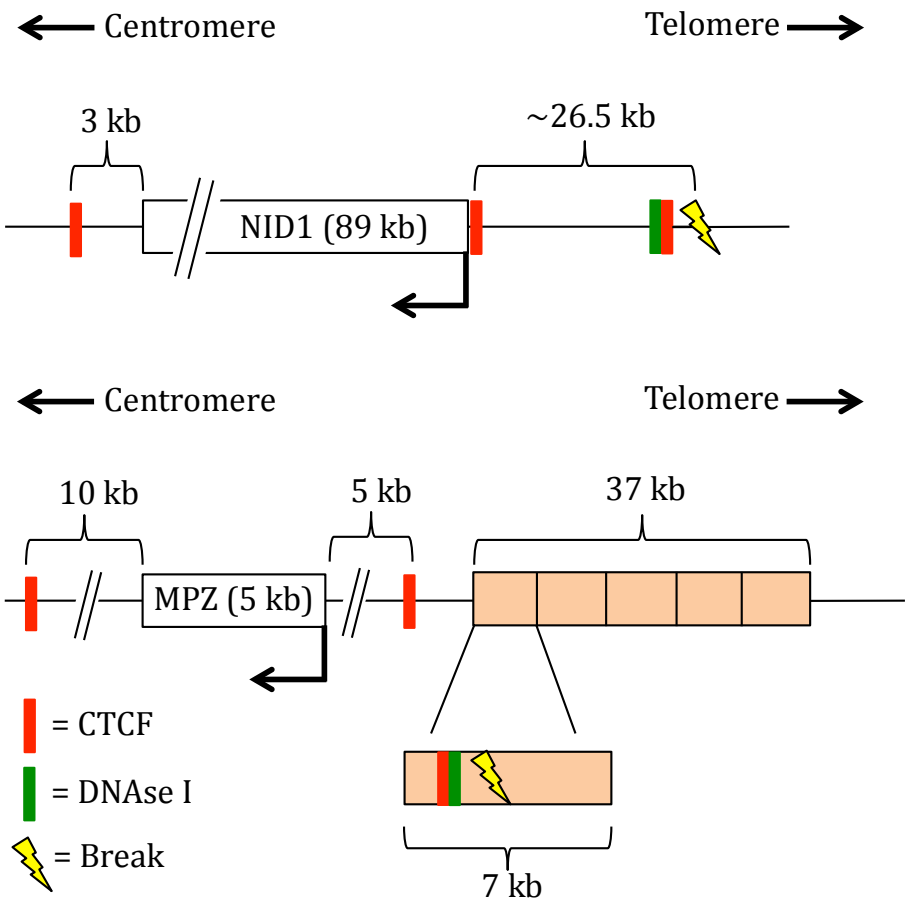

Figure 3: Diagram of the locus surrounding the 1q42 break site (top) and 1q23 break site (bottom). The sites are strikingly similar and both contain CTCF binding sites and DNAse hypersensitivity sites.

Transcriptional Down Regulation Caused by HCMV

Preliminary data shows there is transcriptional down regulation of the NID1 gene at 1q42 during infection, while other adjacent genes LysT (~480,000 bp 5') and GPR137B (~165,000 bp 3') appear unregulated (Figure 4a). Likewise, the data shows

transcriptional down regulation of the MPZ gene at 1q23 (not shown). Temporal bones stained for NID1 (Figure 4b) and MPZ (not shown) show down regulation in infected samples. The down regulation of these proteins in infected clinical samples could contribute to sensorineural hearing loss that is common in infected infants. NID1 and MPZ are important in underlying nerve tracts and providing myelination for nerves in the temporal bone, respectively, and these may both be very important in the hearing loss pathogenesis of HCMV infection.

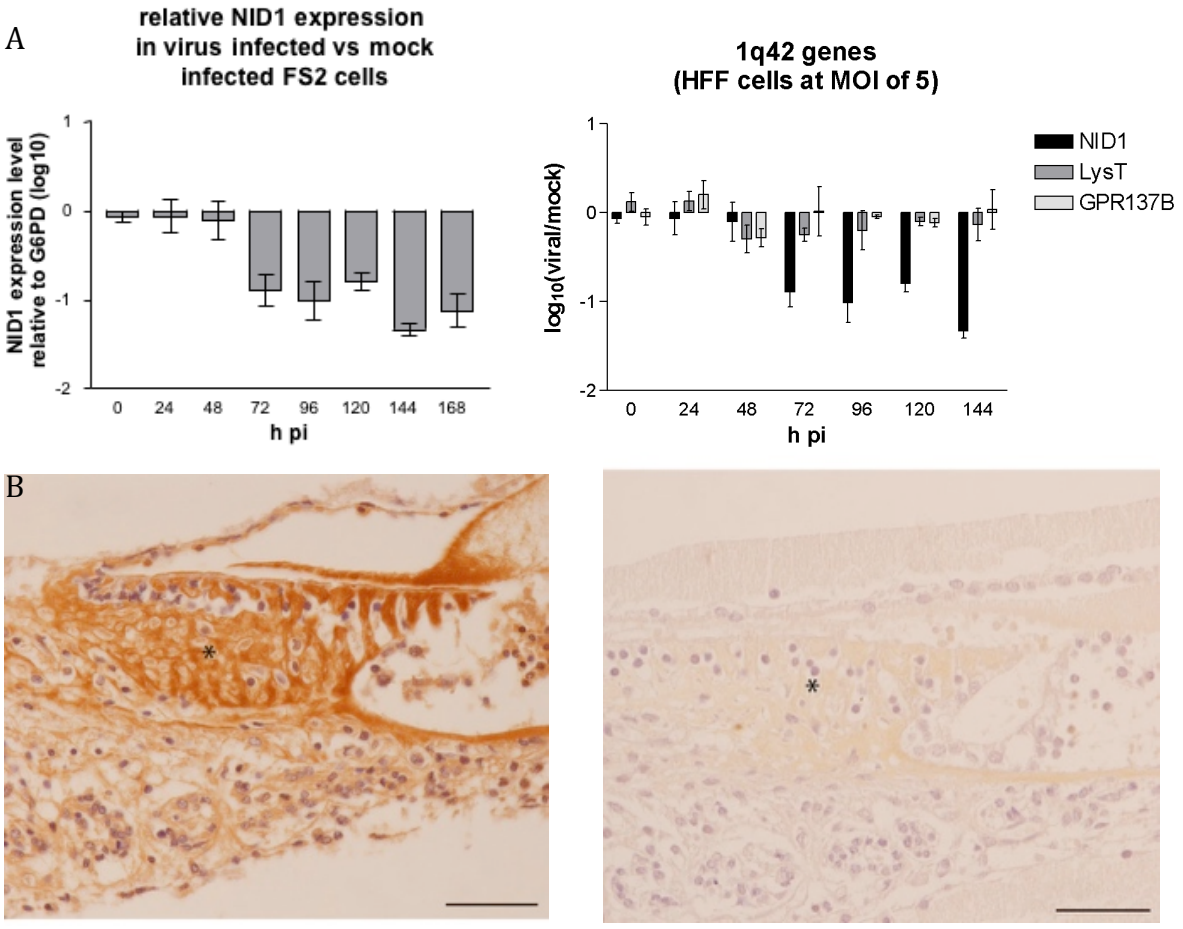

Figure 4: (A) RT-PCR shows an 8-10 fold down regulation of NID1 in infected fibroblasts over a time course of infection (left). Other genes in the surrounding region appear to be un-regulated upon infection (right). Data courtesy of Holger Hannemann. (B) Nidogen staining in normal (left) and infected (right) temporal bones. Asterisks indicate the basement membrane staining around the support cells of the organ of Corti.

Nidogen-1

Nidogen-1 (also known as entactin-1) is an essential and ubiquitous basement membrane protein that is present in the pial membrane, cochlea, and vestibular organs (Ishiyama et al. 2009). Basement membranes are not only important for cell adhesion, but also regulate cell growth, differentiation, migration, tissue development, and repair (Vasudevan et al 2010). Nidogen-1 serves as a stabilizing bridge between layers of laminin and collagen IV that form the scaffold of the basement membrane (Dong et al. 2002). Mice with a targeted deletion of the nidogen-1 binding site of laminin have fragile pial membranes that are disintegrated in random sections. In these regions, radial glia are retracted from the pial surface and migrating neurons either pass the meninges or prematurely end their migration into the cortical plate (Halfter et al. 2002). In the peripheral nervous system, nidogen-1 induces process formation, prevents death, increases proliferation, and induces migration of Schwann cells (Lee et al. 2007). It also induces neurite growth of adult dorsal root ganglia neurons via the interaction of Schwann cells and neurons (Lee et al. 2009). Mutations in NID1 are linked to Autosomal Dominant Dandy Walker Malformation, resulting in brain deformation and neurological defects (Dabro et al. 2013). NID1 knockout mice show behavioral patterns that suggest neurological defects. These behaviors included involuntary movements that resemble a seizure, rigid extension of the legs upon brief exposure to CO_2, a twisted posture and flailing movements when lifted by the tail, and temporarily paralyzed hind legs upon release (Dong et al. 2002).

Myelin Protein Zero

Myelin protein zero is a myelin sheath protein found surrounding cochlear and vestibular nerves in the temporal bone. It is made by Schwann cells, which are exclusively located in the peripheral nervous system (Wang et al. 2013). Myelinating Schwann cells wrap around axons of neurons to form the myelin sheath. Mutation of MPZ is linked to Charcot Marie Tooth Syndrome Type 1B (CMT1B) with sensorineural hearing loss (Su et al. 1993).

CTCF

CTCF is a DNA binding protein that is highly conserved among vertebrates and is ubiquitously expressed in most cell types. It primarily acts as an insulator by blocking the interaction between enhancers and promoters and can also bind DNA strands together, form chromatin loops, and promote the interaction of enhancers and promoters. It regulates the 3D structure of the chromatin and defines the boundaries between active and heterochromatic DNA (Ong and Corces 2014).

CTCF is responsible for the switch between latent and lytic infection in some herpesviruses (HSV-1 and EBV). During latent infection of HSV-1, lytic genes are repressed and a latency-associated transcript (LAT) is produced. During latency, the HSV-1 genome is organized into transcriptionally active regions (corresponding to the LAT) and transcriptionally repressed regions (corresponding to lytic genes). Between these two areas of active and repressed transcription, there is a cluster of CTCF binding factor motifs. CTCF binds to these sites on the latent genome and establishes a

chromatin boundary between latent and lytic genes (Amelio et al. 2006). In latent Epstein Barr Virus (EBV) infection, a small number of viral genes are expressed that are essential for viral genome persistence and cell survival. There are different latency types that are characterized by the pattern of gene expression. CTCF binding sites are located between the origin of EBV replication (oriP) and the Cp promoter. The Cp promoter directs the transcription of the EBNA genes, which are expressed during latent infections. The oriP enhancer regulates Cp transcription. This suggests that CTCF insulates the oriP enhancer from interacting with the Cp promoter during lytic infection (Chau et al. 2006).

CTCF can also negatively regulate major immediate early (MIE) gene expression during HCMV infection. Infected cells produce higher levels of CTCF mRNA and protein. Depletion of CTCF results in an increase in immediate early and early gene expression, as well as virion production. CTCF binds directly with the DNA in the first intron of the MIE gene and blocks interaction of RNA polymerase II function during the early stages of viral transcription (Martinez et al. 2014). It is possible that a viral protein is interacting with CTCF at the break sites or directly with the DNA, causing damage.

Primary Infection vs. Reactivation

Primary maternal infection, as well as reactivation events, can cause transmission from mother to fetus through the placenta. Primary infection during pregnancy is characterized by conversion from serum antibody negative to serum antibody positive. It can also be detected through circulating IgM antibodies to HCMV (Dollard et al. 2011).

Like other herpesviruses, HCMV can cause a lifelong latent infection in the host with periodic reactivation (Nelson and Demmler 1997). Non-primary infection is characterized by reactivation of a latent infection or by reinfection with a new strain (Boppana et al. 2001). Primary infection can occur through sexual activity and through contact with children in a caregiving environment. Primary infection before conception carries the lowest risk of transmission to the fetus and infection during the third trimester carries the highest risk of transmission to the fetus (Pass et al. 2005). Although the risk of transmission to the fetus is much lower in the first and second trimester, the risk of congenital defects is much higher if the fetus is infected during this time (Pass et al. 2005). Mother-to-child transmission following primary infection ranges from 14-52% (Gabrielli et al. 2012).

Normal Development of the Placenta

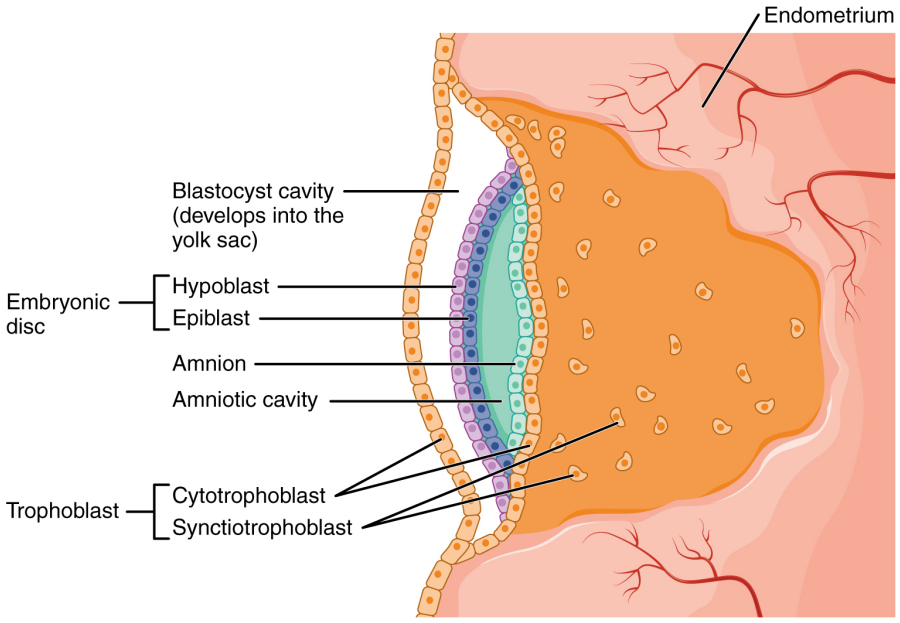

Figure 5: The trophoblast of the implanted human blastocyst differentiates into the inner cytotrophoblast and the syncytiotrophoblast. The syncytiotrophoblasts form villi that participate in transplacental exchange of materials, such as oxygen. Reprinted from OpenStax, Embryonic Development. OpenStax CNX. Jun 4, 2013 http://cnx.org/contents/1704097d-1012-4798-8ef6-1598d73e7b15@3.

After fertilization, the human oocyte undergoes a series of cell divisions to create a sphere of undifferentiated cells called the morula. Upon the formation of the blastocoel cavity, a fluid filled cavity in the center of the morula, it is referred to as a blastocyst. When the blastocyst enters the uterus, it "hatches" out of the zona pellucida, a glycoprotein membrane that surrounds the plasma membrane of the oocyte (Hardy et al. 1989). After the zona pellucida is shed, the underlying layer of trophectoderm replaces it. This trophoblast is the outermost layer of tissue that forms the wall of the blastocyst and it functions in the implantation of the blastocyst in the uterine wall (Figure 5) (Zhou et al. 1997). At implantation, the trophoblast layer is exposed to the lining of the uterus called the endometrium. The trophoblast differentiates into two layers: the inner cytotrophoblast, which forms the chorion, and the syncytiotrophoblast, which develops into the outer layer of the placenta (Figure 5). The

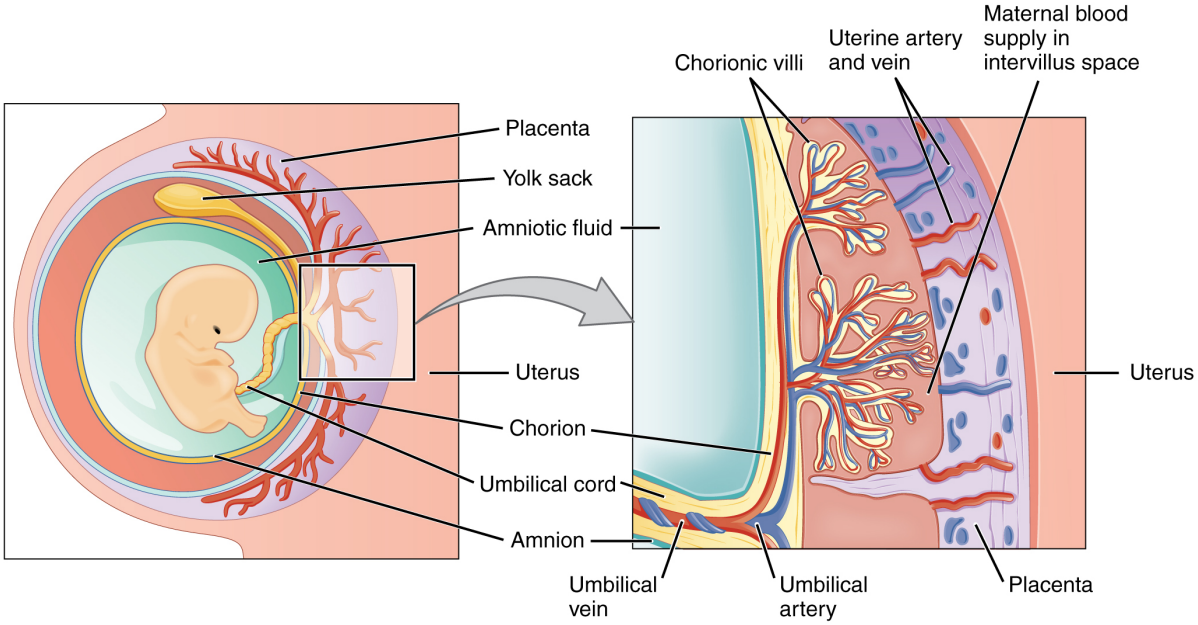

Figure 6: Diagram of the human placenta. Maternal blood flows into the intervillous space through maternal blood vessels and bathes the chorionic villi. Fetal blood enters through the umbilical artery and flows through the embryonic blood vessels contained within the chorionic villi. Reprinted from OpenStax, Embryonic Development. OpenStax CNX. Jun 4, 2013 http://cnx.org/contents/1704097d-1012-4798-8ef6-1598d73e7b15@3.

syncytiotrophoblast is formed by the fusion of mono-nucleated cytotrophoblasts and is in direct contact with maternal tissue (Zhou et al. 1997). The inner layer of cytotrophoblasts that have not made contact with maternal tissues act as stem cells to guarantee growth of the trophoblast by continuous proliferation (Benirschke and Kaufmann 2000). After the trophoblast attaches to the endometrium, it lyses the endometrial surface and continues to penetrate until it is surrounded by endometrium. The endometrial tissue is called decidua during pregnancy and participates in the exchange of nutrients, gas, and wastes during gestation (Gude et al. 2004). Primary chorionic villi are formed by evaginations of the syncytiotrophoblast that contain a cytotrophoblast core. By the third week of gestation, fetal capillaries form within these villi and project into the space where maternal blood circulates known as the intervillous space (Figure 6) (Gude et al. 2004). The villi participate in transplacental exchange of materials, such as oxygen, primarily via passive diffusion (Mayhew 2003).

HCMV Infection of the Placenta

Trophoblast cells, the specialized epithelial cells of the placenta, are thought to be the first target for maternal HCMV. Trophoblast cells transport a wide variety of substances to the fetus, including maternal IgG via the Fc receptor. HCMV virions coated with maternal IgG antibodies specific to viral glycoproteins can undergo transcytosis to the cytotrophoblast layers underneath the syncytiotrophoblast layer (Fisher et al. 2000). Previous work has shown that human cytotrophoblasts are fully permissive for HCMV *in vitro* and that they play an important role in the transmission of virus to the fetus. Additionally, the virus may enter through the intervillous space where direct

dissemination of the virus from maternal blood to the cytotrophoblasts of the floating villi can occur. Infected macrophages located among decidual granular leukocytes are another potential route of infection. Infectious cells in the maternal blood can also encounter endothelial cells and the endovascular cytotrophoblasts. Later in infection, syncytiotrophoblasts may also become infected. Placental HCMV infection has been detected in the presence and absence of fetal infection, suggesting the placenta is an important site of either transmission or protection from infection (Maidji et al. 2002).

Widespread necrosis is found in placental HCMV infection (Gabrielli et al. 2012). Infection arrests early differentiation stages involving the development of human trophoblastic progenitor cells (TBPCs). These progenitor cells eventually give rise to mature cells of the chorionic villi, such as syncytiotrophoblasts and invasive cytotrophoblasts that remodel uterine vasculature. Viral antigens are also present in TBPCs of the chorion in clinical cases of congenital infection. Chorions from symptomatic congenital infections contained significantly fewer cells positive for GATA4, a marker of TBPCs. This suggests that infection reduces the number of TBPCs available to differentiate into mature chorionic villi cells (Tabata et al. 2015). *In vitro*, HCMV replicates in TBPC lines derived from the chorion and alters expression and localization of proteins involved in pluripotency, early differentiation, and cell cycle progression. In primary cytotrophoblasts, HCMV infection hinders late stages of differentiation and invasion (Tabata et al. 2012).

Brain Abnormalities of Congenitally Infected Infants

Congenital brain defects can be seen via neuroimaging, such as MRI or CT scan. Intracranial calcification is the most frequently reported finding in congenital HCMV imaging (Figure 7a). The calcifications are most commonly located in periventricular regions and are thick and chunky, but can also be located in other areas, such as the basal ganglia (de Vries et al. 2004). Presence of calcifications is associated with developmental delays and mental retardation, but not all patients show cerebral calcifications (Noyola et al. 2001). Some patients with normal neurological function have calcification related to congenital HCMV infection (Zucca et al. 2003).

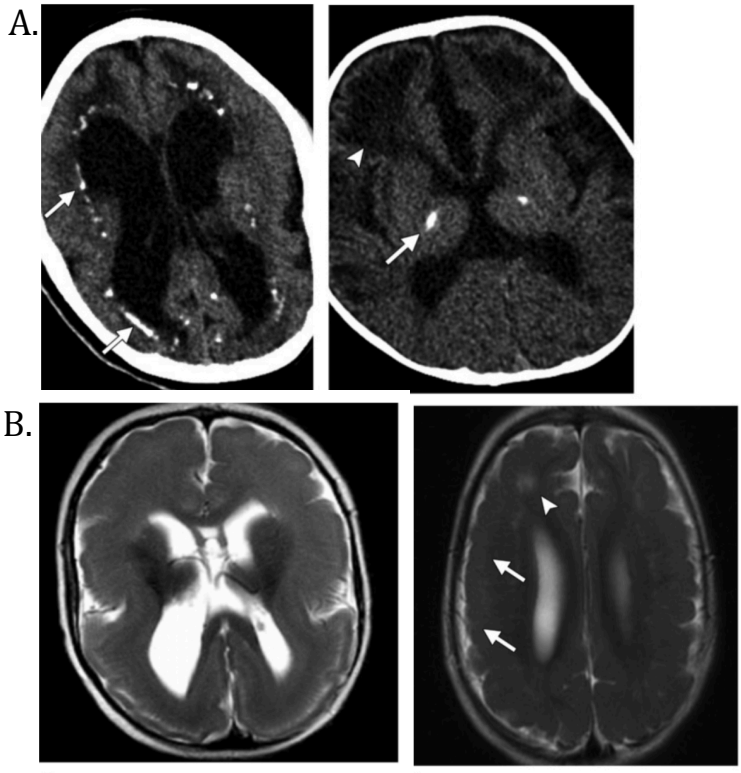

Figure 7: Congenital brain defects caused by HCMV can be seen via neuroimaging. (A) Cerebral calcifications are most commonly located in periventricular regions (left), but can also be found in the basal ganglia (right). (B) Migrational abnormalities such as lissencephaly (left) and pachygyria (right) can also be seen. Both of these give the brain a smooth appearance due to a lack of gyri and sulci. Reprinted by permission from RSNA: Radiographics (Fink et al.), copyright 2010.

Various migrational abnormalities have been reported in patients with congenital HCMV infection that can be seen via neuroimaging (Figure 7b). These abnormalities can include lissencephaly in which the brain surface lacks sulcation, giving the brain a "smooth" appearance. Patients can also exhibit pachygyria, in which gyri are broad and only partial sulcation is present. Polymicrogyria may resemble an area of thickened cortex without a normal gyri pattern, but in reality there are small and abnormal gyri present (Fink et al. 2010). Both lissencephaly and pachygyria are associated with a worse neurological outcome than that associated with polymicrogyria and their presence indicates early fetal infection (Hayward et al. 1991).

White matter abnormalities are also common in congenital HCMV infection. In MRI images, white matter disease appears as areas of hyperintensity relative to adjacent, normal white matter (Fink et al. 2010). White matter disease indicates delayed myelination of neurons (van der Knaap et al. 2004). Although this feature is common in congenital HCMV disease, it is also present in a variety of other neurological conditions. The presence of periventricular cysts adjacent to the ventricles has also been reported in patients with congenital HCMV infection (de Vries et al. 2004). They are particularly common adjacent to the anterior temporal lobes and are often associated with white matter abnormalities (de Vries et al. 2006). Cysts associated with white matter disease are somewhat specific for HCMV infection (van der Knaap et al. 2004). Other notable findings via neuroimaging include ventricular adhesions (Zucca et al. 2003) and cerebral atrophy. Abnormal dilation of the lateral ventricles, called ventriculomegaly, as

well as an abnormally small brain and head, called microcephaly (Figure 8), are major causes of cerebral atrophy (Noyola et al. 2001).

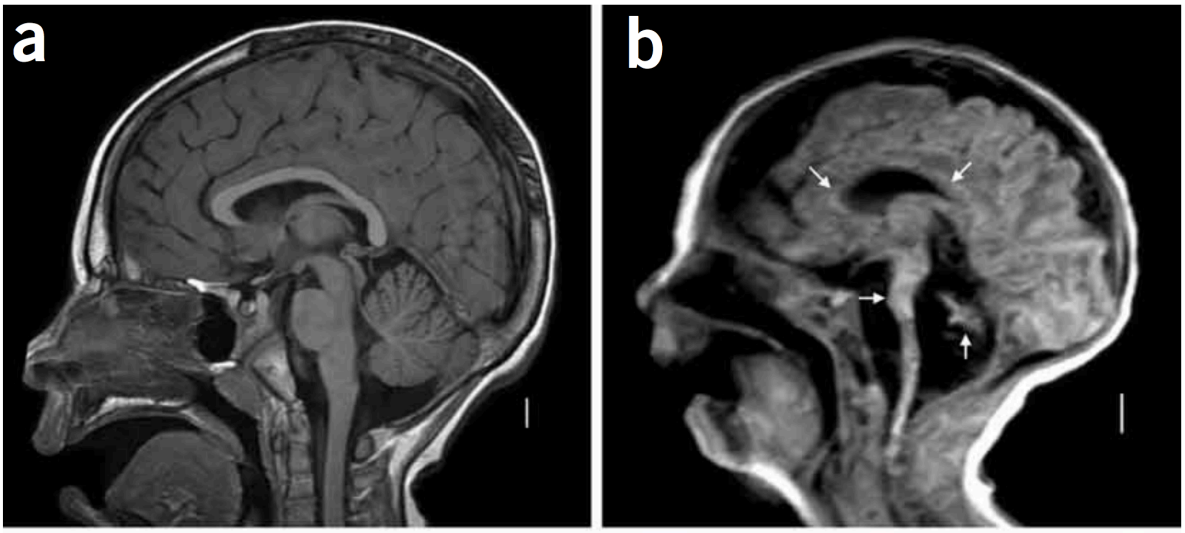

Figure 8: Microcephaly is a common defect among infants congenitally infected with HCMV. Patients with microcephaly have an abnormally small brain and head (B) compared to normal infants (A). Reprinted from Macmillan Publishers Ltd: Nature Genetics (Najm et al.), copyright 2008.

The density of HCMV infected cells is correlated with the extent and severity of brain abnormalities (Teissier et al. 2014). Focal regions of necrosis found in infected brains are frequently associated with inflammation, apoptotic cells, and HCMV positive cells. Brain tissue with low viral loads shows a weak inflammatory response and is associated with less severe brain damage. Brain tissue with high viral loads shows infiltration of $CD8^+$ T cells, which could be responsible for immune mediated damage (Gabrielli et al. 2012).

Previous studies have shown that cells within the sub-ventricular zone (SVZ) of congenitally infected infants are preferentially infected by HCMV (Chang et al. 2002 and Kawasaki et al. 2002). The SVZ lies on the periphery of the lateral ventricles and participates in neurogenesis of the developing brain. It provides a source of NPCs and

neural stem cells that can migrate, proliferate, and differentiate into neurons and glia (Gage 2000). As the NPCs differentiate, they migrate along radial glia away from the lateral ventricles and toward the pial surface of the brain (Figure 9). The pial surface is rich in basement membrane proteins (such as nidogen-1) that radial glia anchor themselves to (Ishiyama et al. 2009). If the basement membrane of the pial surface is compromised, the radial glia retract and neurons are not able to properly migrate into the cortical plate (Halfter et al. 2002). Infection of cells in the SVZ may contribute to the appearance of migrational abnormalities in the brain (lissencephaly and pachygyria) as well as microcephaly.

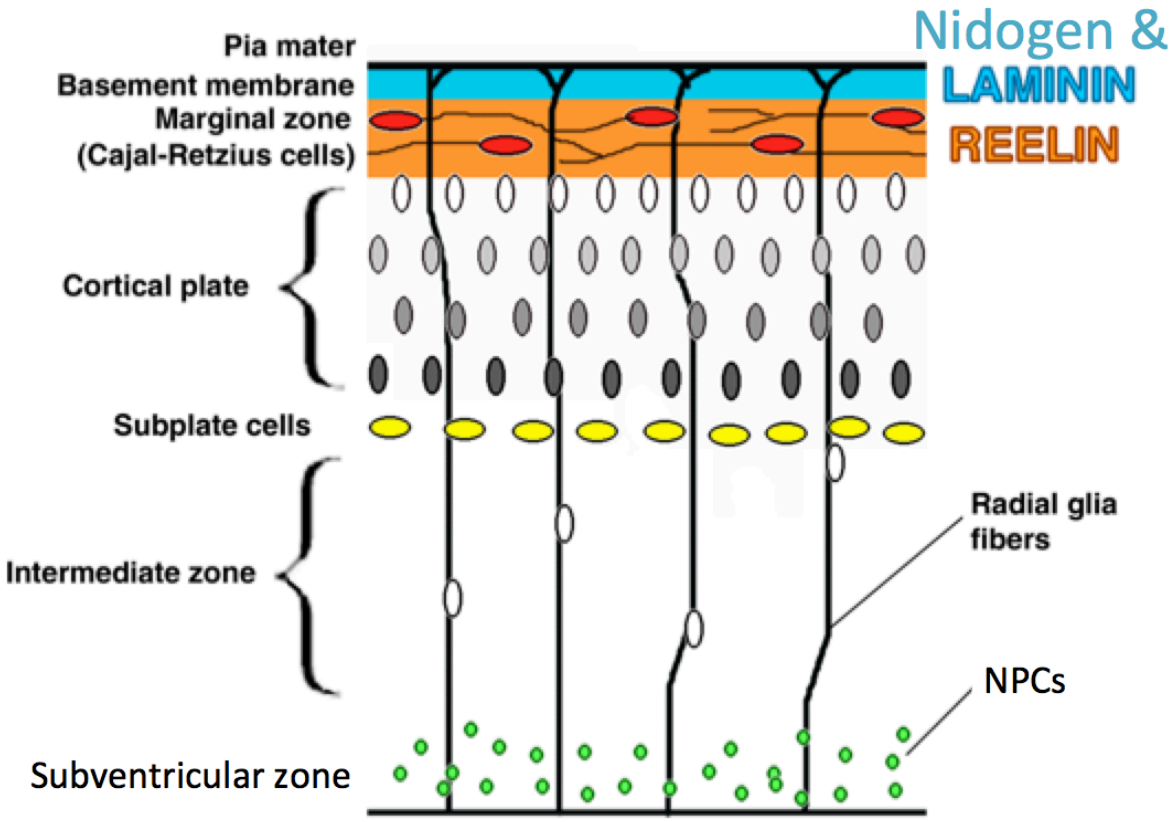

Figure 9: Neural progenitor cells (NPCs) in the sub-ventricular zone (SVZ) migrate along radial glia fibers from the ventricular surface towards the pial surface as they differentiate. The pial surface is rich in basement membrane proteins, such as nidogen-1. Adapted from diagram found at: https://en.wikipedia.org/wiki/Corticogenesis.

HCMV Induced Sensorineural Hearing Loss

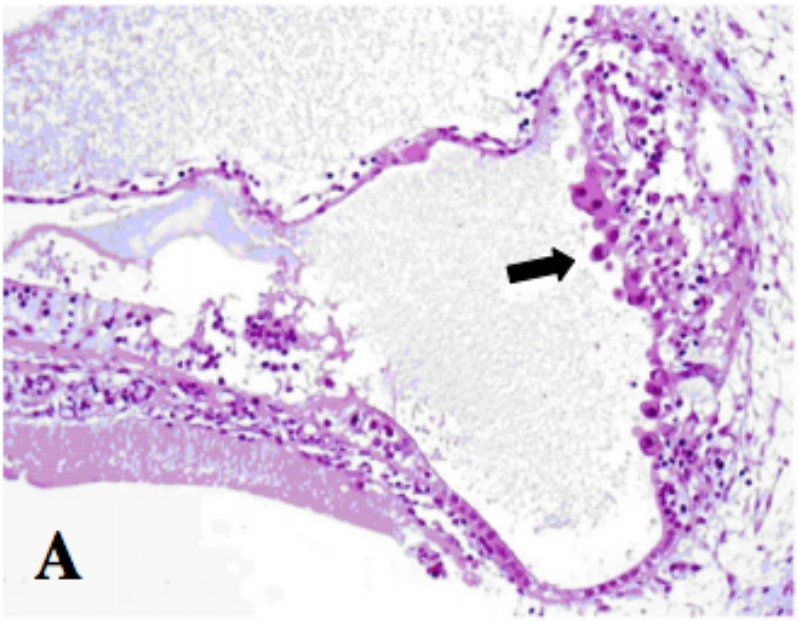

Figure 10: Lesions of the inner ear are common in congenital HCMV infection and include cytomegalic cells, as well as inflammation. The lesions are present in the cochlea, the supporting cells of the organ or Corti, non-sensory epithelial cells, and in the vestibular apparatus. Arrow points to cytomegalic inclusions in the marginal layer of the vascularis. Reprinted from BioMed Central: Acta Neuropathologica (Gabrielli et al. 2013).

Sensorineural hearing loss is the most common symptom related to congenital HCMV infection. Hearing loss can be unilateral or bilateral and can range from mild to severe (Gross et al. 2007). Inner ear lesions are common and possibly contribute to widespread sensorineural hearing loss. Lesions of the inner ear include cytomegalic cells as well as inflammation (Figure 10). These lesions are present in the marginal cells of the stria vascularis of the cochlea, which provide endolymph for the scala media and is involved in potassium ion transport. Infection of these cells may alter ion circulation and consequently affect hearing (Gabrielli et al. 2013). Infection is also present in the supporting cells of the organ of Corti, in non-sensory epithelia of the inner ear, and in the vestibular apparatus (Teissier et al. 2011).

Animal Models of HCMV Infection

Murine CMV (MCMV) and host susceptibility is the best characterized animal CMV. Unlike HCMV, MCMV is unable to cross the placenta of pregnant mice and must be injected into the placenta or fetus mid-gestation. Using these methods of infection, there is a high degree of fetal loss (Melnick and Jaskoll 2013). The embryos that do survive show growth retardation, brain infection, and microcephaly (Li and Tsutsui 2000). Infected cells of the brain are predominantly located in the ventricular and sub-ventricular zone (Kawasaki et al. 2002). MCMV seems to target neural stem cells and NPCs residing in these regions, causing a loss of neurons and disturbing neural migration. Infection of neural stem cells and NPCs results in down-regulation of multipotency factors and neural identity genes (Mutnal et al. 2011). Disruption of neuron migration has also been observed in mice postnatally infected with MCMV (Shinmura et al. 1997). Infected neurons in the cortex can persist and produce low levels of virus, suggesting they can provide a long-term reservoir of virus in the developing brain (Kosugi et al. 2002).

Guinea pigs are also frequently used to study the impact of congenital CMV infection. Like HCMV, guinea pig CMV (GPCMV) is able to cross the placenta and infect the fetus *in utero*. The structure and histology of the guinea pig placenta is very similar to humans, with a single trophoblast layer separating the maternal and fetal blood supply. This makes the guinea pig model system well suited to study how the virus crosses the placenta and how it can be prevented (Schleiss and McVoy 2010). The cochlea can be infected by GPCMV *in utero*, as well as by direct infection of the inner ear. Direct

injection of GPCMV into the inner ear of adults, as well as vertically infected animals, have cellular abnormalities of the cochlea and hearing loss (Katano et al. 2007). Although these animal models are very useful for investigating the pathogenesis of species specific CMVs, we need to study HCMV in human cells.

ESCs and iPSCs as a Model for Congenital HCMV Infection

Advancements in the field of human pluripotent stem cell culture allow researchers to study HCMV infection in a medically relevant system. Pluripotent stem cells have the ability to differentiate into all adult cell types, including neurological cell types such as neurons and glia. Two different sources of pluripotent cells have been used to study HCMV infection, embryonic stem cells (ESCs) and induced pluripotent stem cells (iPSCs). ESCs are pluripotent cells that have been harvested from the inner cell mass of a human blastocyst, while iPSCs are adult somatic cells that have pluripotency genes OCT4, KLF4, SOX2, and c-Myc introduced via a viral vector (Takahashi and Yamanaka 2006). Undifferentiated ESCs and iPSCs are susceptible to HCMV, but not permissive. This means that the virus can bind and enter the cells, but there are no *de novo* viral antigens expressed and the virus does not replicate (D'Aiuto et al. 2012). Primitive neural stem cells can harbor viral genomes and are possibly a reservoir for the virus in the fetal brain (Belzile et al. 2014). Neural precursor cells (NPCs) derived from iPSCs are fully permissive to HCMV infection (D'Aiuto et al. 2012 and Penkert and Kalejta 2013). Neonatal NPCs, neurons, and glia derived from NPCs are fully permissive to HCMV infection (Luo et al. 2008). Infected neonatal NPCs undergo premature and

abnormal differentiation. Multipotency genes and neural identity genes are down regulated in these infected NPCs (Luo et al. 2010).

Neurons derived from pluripotent stem cells stain positive for beta tubulin III in a very distinct pattern. Beta tubulin III is present in the axon of neurons and immunofluorescence staining shows long neuronal projections. Infected neurons show abnormal beta tubulin III morphology when compared to uninfected neurons (Figure 11). The projections of beta tubulin appear to be truncated in infected cells and

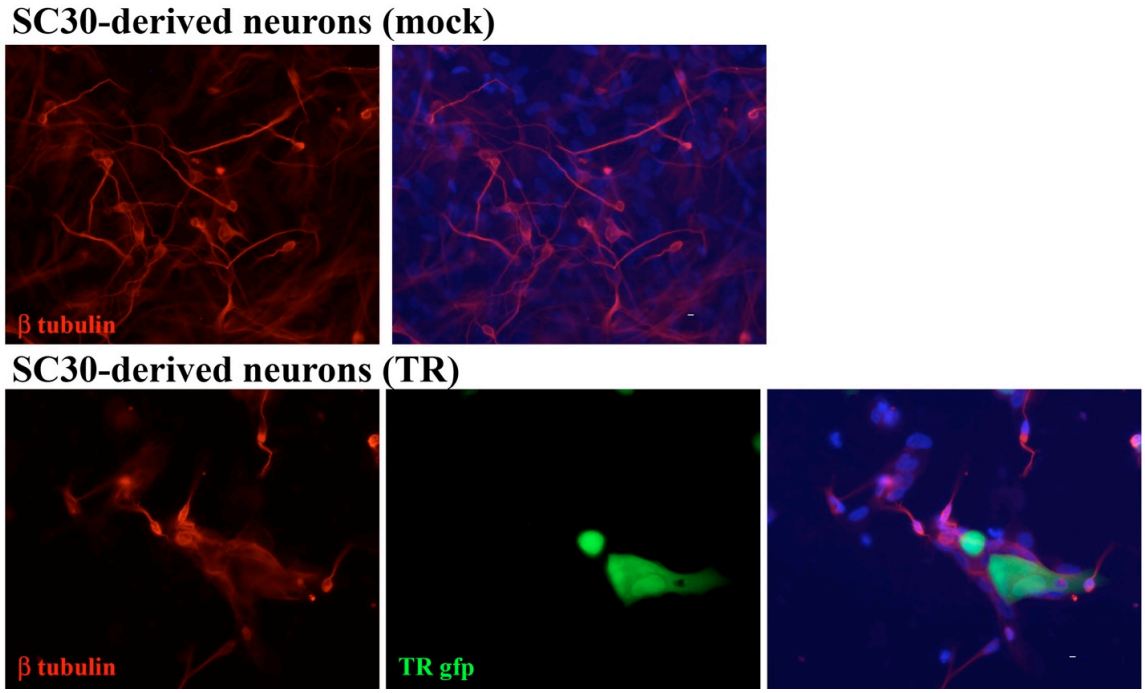

Figure 11: Uninfected iPSC-derived neurons show elongated projections of beta tubulin III (top). iPSC-derived neurons infected with a recombinant GFP virus show many areas of shortened beta tubulin III projections and aberrantly stained cells (bottom). These areas often surrounded GFP-positive cells.

adjacent to infected cells. This suggests that HCMV impairs neuronal differentiation in neural stem cells (D'Aiuto et al. 2012, Belzile et al. 2014, and Luo et al. 2010).

Cerebral Organoids

Infected pluripotent cells have been differentiated into various cell types of the brain via the 2D culture system. Although neurons and glia derived from ESCs and iPSCs are a more clinically relevant infection model, it does not mimic the architecture and environment of the brain. The cells are cultured as an adherent monolayer on an artificial matrix. This makes it impossible to study structural characteristics that are present in the brain.

Cerebral organoids, a three-dimensional brain development model that utilizes pluripotent stem cell growth and differentiation, were originally developed to study microcephaly in patient-derived iPSCs (Lancaster et al. 2013). The organoids have cerebral-like structures that resemble the SVZ of a developing brain. Within these

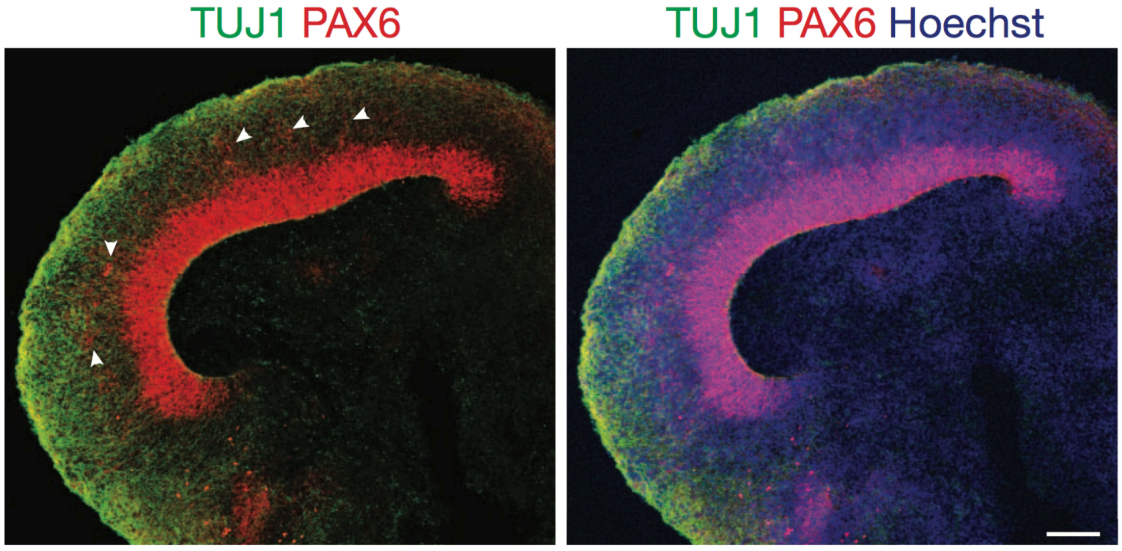

Figure 12: Previously described cerebral organoids (Lancaster et al. 2013) have internal cerebral-like structures. The pattern of NPC (PAX6) and neuron (TUJ1) markers resembles the SVZ of the developing brain. Reprinted by permission from Macmillan Publishers Ltd: Nature (Lancaster et al.), copyright 2013.

structures, cells stain positive for PAX6, an NPC marker. Around the outer and inner rim of the cerebral structures, cells stain positive for beta tubulin III (TUJ1), a neuron marker (Figure 12). The pattern of NPC and neuron markers within the structures suggests that the NPCs are differentiating and migrating to the periphery, much like NPCs of the SVZ in the developing brain (Lancaster et al. 2013). Cerebral organoids could be a valuable tool to study how HCMV affects brain development at very early time points that can't bee seen using clinical samples or 2D cell culture. This work will be described in detail in chapter three.

CHAPTER 2: SPECIFIC DNA DAMAGE INDUCED BY HCMV INFECTION

Introduction

HCMV-induced Chromosome One DNA Damage and Repair

HCMV causes site-specific breaks on chromosome one at 1q42 and 1q23 (Fortunato et al. 2000). Breaks can occur at each site alone or at both simultaneously (Figure 1A) and occur as early as 15 minutes pi (Figure 1B). At 24 hpi, 30% of infected fibroblasts are broken at the 1q42 locus, declining to 15% over 120 h. A decline in the frequency of breaks over 120 h suggests the DNA is being repaired. UV-inactivated (transcriptionally inactive) virus also breaks the DNA, meaning the viral candidate protein contributing to DNA damage is not synthesized *de novo*, but rather is brought in with the virus. Improper DNA repair at these break sites could introduce mutations, which are detrimental to the development of the fetus and can potentially lead to the down-regulated expression of break site-encoded genes. Although the break sites have been broadly mapped and characterized via cosmid clone mapping, the exact locations remain unclear. Further characterization at these loci is needed to understand how viral proteins may be interacting with the DNA. Previous work has shown that during infection, viral DNA is preferentially repaired over host DNA (O'Dowd et al. 2012). Although no physical gaps remain, breaks may be repaired incorrectly. FISH can only detect large-scale DNA damage and there may be multiple breaks occurring at either break site that can't be detected using this method. The DNA could be constantly broken and repaired, causing additive damage. In this study, we set about to more finely map the 1q42 locus in order to determine the extent of damage and whether or not the apparent repair we observed was accurate or mutagenic.

Materials and Methods

Cells and Virus Growth

FS2 primary foreskin fibroblasts were isolated from tissue and propagated in Eagle's minimal essential media (MEM) supplemented with 10% heat inactivated fetal bovine serum (FBS), L-glutamine (2 mM), penicillin (200 U/mL) and streptomycin (200 µg/mL). Cells were grown and maintained at 37˚C and 5% CO_2. The Towne strain of HCMV was obtained from the ATCC (#VR 977), propagated under standard procedures (Tamashiro et al. 1982), and used at a multiplicity of infection (MOI) of 5.

Cell Synchronization and Infection

The medium on actively dividing cells was exchanged for one without serum or supplements for ~60 hours to synchronize the cells. The cells were then trypsinized and re-seeded in 10 cm plates at 5 x 10^5 cells per plate. Cells were allowed to attach to the plate and were then infected at an MOI of 5. Cells were collected at one hpi.

Ligation Mediated PCR (LM-PCR)

In order to finely map chromosome one break sites introduced by HCMV, we used ligation mediated PCR (LM-PCR) (Kong and Maizels 2001) (Figure 13). Genomic DNA from infected fibroblasts was harvested via GeneJET Genomic DNA Purification Kit (Thermo Scientific). Because breaks occur as early as 15 min pi and the frequency of breaks does not begin to decline until 48 h later, we could harvest cells at a very early time pi (1 hpi). Two oligonucleotides were ligated together to create a small

oligonucleotide linker with one blunt and one staggered end. Biotinylated primers were designed in 1 kb increments across the break site region previously identified with cosmid clones (Figure 14). The genomic DNA was denatured in the presence of the biotinylated primers, followed by primer extension. Extension terminated at a break in

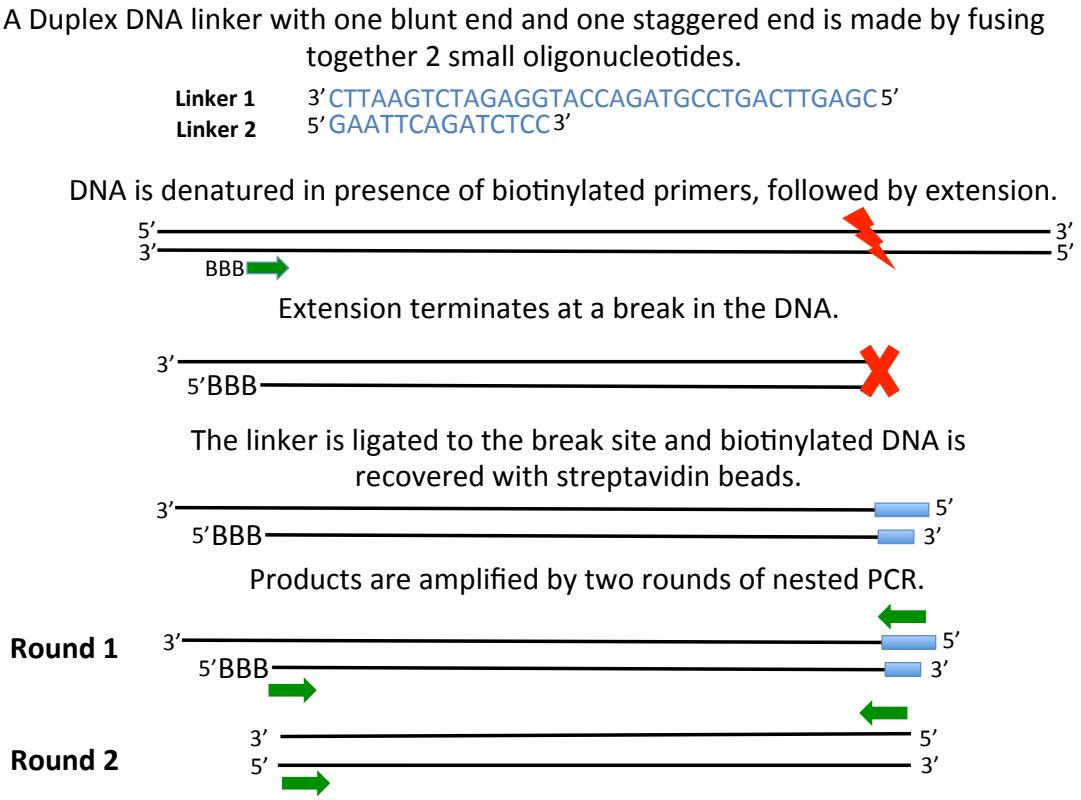

Figure 13: Break site LM-PCR protocol flowchart. Method is described in the text.

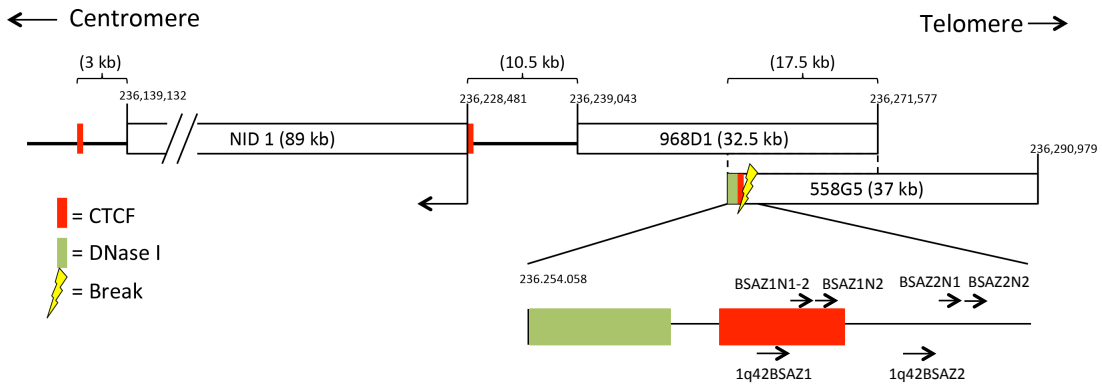

Figure 14: LM-PCR primers with respect to the cosmid clones previously used to broadly map the break site at 1q42.

the DNA and the DNA linker was ligated to the break end. The biotinylated DNA was recovered with streptavidin beads. Two rounds of nested PCR were performed to amplify the biotinylated DNA containing the linker. The PCR products were analyzed via gel electrophoresis. Only the bands that appeared in the HCMV-infected samples and not in the mock-infected samples were considered for sequencing. The PCR products from nested PCR 2 were sequenced and compared to the database sequence (hg38) of this region to determine where specifically the breaks occurred.

The duplex DNA linker was generated by annealing linker 1 (CGAGTTCAGTCCGTAGAC-CATGGAGATCTGAATTC) and linker 2 (GAATTCAGATCTCC), each at 20 μM, in 250 mM Tris pH 8 (Kong and Maizels 2001). The linker was stored at -20˚C. The primers linkerN1 (CGAGTTCAGTCCGTA-GAC) and linkerN2 (GTAGACCATGGAGATCTGAATTC) were used as linker specific primers for the first and second rounds of PCR, respectively (Kong and Maizels). The 5' biotinylated primers 1q42BSAZ1 (GCCTAGAACAGTGCTTGG-CAC) and 1q42BSAZ2 (CACGGGGCCCTTGTCTACATCA) were used in the in primer extension step for the detection of breaks. The resulting PCR product from 1q42BSAZ1 extension was amplified with BSAZ1N1-2 (GAGCACTAGATGTCGGTAAACTATC) and linkerN1 in the first round of nested PCR and BSAZ1N2 (GGATTTGCAGCTGTTAACAGT-CC) and linkerN2 in the second round of nested PCR. The resulting product from 1q42BSAZ2 extension was amplified with BSAZ2N1 (GCATTATCTCCAGGGTGTCACT) and linker N1 in the first round of nested PCR and BSAZ2N2 (GCAGAAAGGGGAGAGAGG-AAGTG) in the second round of nested PCR.

For primer extension, 0.6 pmol biotinylated primer was added to 4000 cell equivalents of DNA in NEB buffer 2 (New England Biolabs) in a total of 15 µL. The DNA was denatured at 95˚C for three minutes and the primer was annealed at 64˚C for 30 minutes. After annealing, 7.5 µL of an ice cold solution containing 0.25 mM dNTPs and 1.5 µL Exo- Klenow Fragment (New England Biolabs) diluted in water was added. Primer extension was carried out at 37˚C for 30 minutes. After extension, 6 µL of cold 0.3 M Tris pH 7.7 was added and the Exo- Klenow Fragment was inactivated by incubation at 75˚C for 20 minutes.

Linker ligation was carried out by adding 45 µL of a cold, freshly made ligation mixture to the extension reaction. The ligation mixture contained 100 µmol of pre-annealed linker1/linker2 in 250 mM Tris pH 8, 400 U of T4 DNA ligase (New England Biolabs), ligation buffer, and water. Ligation was carried out at 16˚C overnight. Extension-ligation products were recovered by the addition of 300 µg of pre-washed MagnaLink Streptavidin Magnetic Beads (Solulink), suspended in 75 µL of 2X bind/wash buffer (10 mM Tris ph 7.3, 1 mM EDTA, 2M NaCl, 0.02% Tween-20) to a final volume of 150 µL. The tubes were then incubated at 43˚C for 1 hour with brief mixing every five minutes. The beads were then pelleted with a magnet and washed twice with bind/wash buffer and once with 10 mM Tris pH 7.5.

Both rounds of nested PCR were carried out in 50 µL reactions containing HotStart-IT Taq Master Mix (Affymetrix). Primer concentration was 100 nM in the first round of PCR and 400 nM in the second round. For the first round PCR, bead-bound extension

products were added to the reaction mix and followed limited PCR (1 cycle: 95˚C for 2 min, 55˚C for 4 min, 72˚C for 3 min; 2 cycles: 95˚C for 45 s, 55˚C for 1 min, 72˚C for 2 min; 1 cycle: 72˚C for 7 min). The beads were removed, the reaction products were transferred to a new PCR tube, and PCR continued (1 cycle: 95˚C for 4 min; 28 cycles: 95˚C for 45 s, 55˚C for 1 min, 72˚C for 2 min; 1 cycle: 72˚C for 7 min). A 2 µL aliquot of first round product was used for the second round of amplification (1 cycle: 95˚C for 4 min; 35 cycles: 95˚C for 45 s, 62˚C for 1 min, 72˚C for 2 min; 1 cycle: 72˚C for 30 min). the PCR products were sequenced and compared to the databases sequence (hg38) of this region to determine where specifically the breaks occurred. The junction between genomic DNA and the linker sequence identified the location of the breaks. This process was repeated multiple times to determine if the breaks were occurring at the same position every time or randomly within the region.

Deep Sequencing

To analyze how breaks in chromosome one affect the DNA sequence, we used deep sequencing to compare HCMV-infected cells and mock-infected cells. Fibroblasts were infected at an MOI of 5 as described above. Four hours after infection, the viral supernatant was removed from the cells and replaced with complete media. Mock and virus infected HFFs were collected at 24, 72, 96, and 120 hpi in the first experiment, as well as two mock and long term-infected neuron time points. In the second experiment, mock-infected cells were collected at 24 hpi and infected cells were collected at 24 and 120 hpi. Genomic DNA was harvested from the cells using the GeneJET Genomic DNA Purification Kit (Thermo Scientific). 1.5 x 10^5 cell equivalents (first experiment) or 1000

cell equivalents (second experiment) were used as the PCR template. Using the break sites mapped with LM-PCR, we designed primers that encompassed all the break sites.

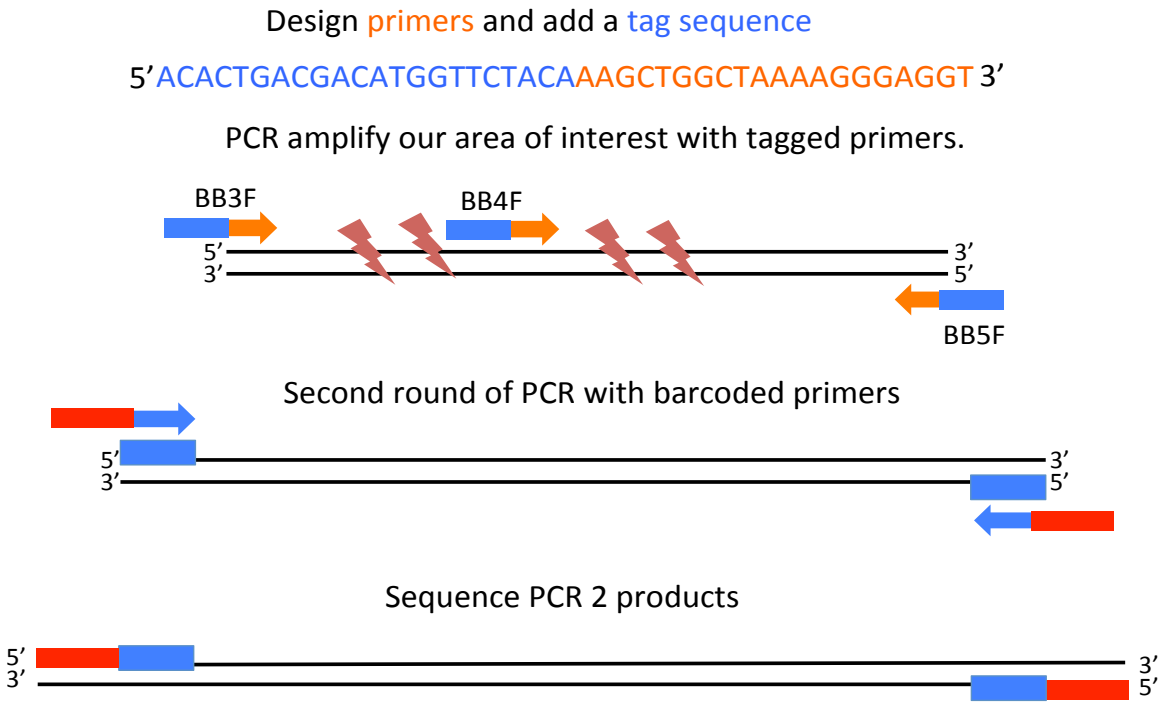

Figure 15: 1q42 break site deep sequencing. A tag sequence was added to the 5' end of the primers designed to amplify the break site region. The resulting PCR product contained the tag sequence. A set of barcoded primers that hybridize to the tag sequences were used to amplify the break site in a second round of PCR.

The resulting amplicons were designed to about 550 bp long in the first experiment and less than 400 bp in the second experiment. A small tag sequence was added to the 5' end of the primers and the resulting PCR product contained the tag sequence. The resulting PCR products were diluted either 1:5 (first experiment) or 1:15 (second experiment). A second round of PCR was conducted with each sample getting a unique barcode primer (provided by iBEST). These primers hybridized to the 5' tag sequence from the first round of PCR. The resulting PCR product was deep sequenced using an Illumina Miseq (Figure 15).

Table 1 lists the primers used for each experiment, their sequences, and the 5' tag sequence added to each primer. In the first experiment, we used two primer pairs that that covered all of the mapped break sites identified using LM-PCR (see figure 18 below). The resulting amplicon from the BB3F/BB5R primer pair was 564 bp long and the amplicon from the BB4F/BB5R primer pair was 342 bp long. In the second experiment, we used three primer pairs to generate shorter products (see figure 19b below). The primer pairs used in the second experiment are as follows: BSAZ2N2/BB7R (374 bp), BB3F/BB4R (417 bp), and BB7F/BSAZ3R (325 bp).

Table 1: Primers and the 5' tag sequences used in the first and second deep sequencing experiments.

	Primer Name	Oligonucleotide Sequence
First Experiment	BB3F	AAGCTGGCTAAAAGGGAGGT
	BB4F	TGGGTTTCTCATCGAGCAGT
	BB5R	CACGCCTGTAATCCCAACAC
Second Experiment	BSAZ2N2	GCAGAAAGGGGAGAGAGGAAGTG
	BB3F	AAGCTGGCTAAAAGGGAGGT
	BB7F	CAGTGTATTGGGTGCCGTTC
	BB7R	GAACGGCACCCAATACACTG
	BB4R	ATCCCAGTTGAGTGAGCCAA
	BSAZ3R	GTGTCCATCCATCAGTAAGAC
Tag Sequences	Forward Tag	ACACTGACGACATGGTTCTACA
	Reverse Tag	TACGGTAGCAGAGACTTGGTCTCA

For the first experiment, we used HotStart-IT Taq Master Mix (Affymetrix) in the first round of PCR amplification. The PCR conditions were as follows: 1 cycle 94˚C for 5 min; 25 cycles 94˚C for 30 s, 58˚C for 30 s, 72˚C for 30 s; 1 cycle 72˚C for 7 min. For the second round of PCR using barcoded primers, we used Q5 Hot Start High Fidelity DNA Polymerase (New England Biolabs) with 0.5 µM primers, 200 µM dNTPs, and 1X Q5 reaction buffer. The PCR conditions were as follows: 1 cycle 95˚C for 1 min; 10 cycles 95˚C for 30 s, 60˚C for 30 s, 68˚C for 1 min; 1 cycle 68˚C for 5 min.

For the second experiment, we used Phusion Flash PCR Master Mix (Thermo Scientific) with 0.5 μM primers in the first and second round of PCR amplification. We used a different annealing temperature for each primer pair in the first round of amplification. Table 2 lists the annealing temperature for each primer pair. The PCR conditions were as follows: 1 cycle 98˚C for 10 s; 30 cycles 98˚C for 5 s, x˚C for 5 s, 72˚C for 15 s; 1 cycle 72 ˚C for 1 min. For the second round of PCR using barcoded primers, the PCR conditions were as follows: 1 cycle 95˚C for 1 min; 10 cycles 95˚C for 30 s, 60˚C for 30 s, 68˚C for 1 min; 1 cycle 68˚C for 5 min.

Table 2: Experiment two annealing temperatures for each primer pair in the first round of PCR amplification.

Primer Pair	Annealing Temperature
BSAZ2N2/BB7R	62˚C
BB3F/BB4R	60˚C
BB7F/BSAZ3R	61˚C

HCMV vs. Break Site Sequence Comparison

We used the Basic Local Alignment Search Tool (BLAST) to compare the whole HCMV Towne genome (accession number FJ616285.1) to the 1q42 and 1q23 break site regions. Matches of high similarity (80-100%) were mapped on the break site regions and the HCMV genome. Matches on 1q42 and 1q23 were compared with each other to determine if there were common sequences. The locations of sequence homology on the HCMV genome were analyzed to determine which gene (or regulatory element) it fell within. To determine a “baseline” of sequence similarity, we compared the HCMV genome to similar regions that contained a CTCF binding region, but were not broken upon infection. We also compared the break site regions to the genomes of EBV

(accession number NC_007605.1) and HSV-1 (accession number X14112.1) that don't cause DNA damage during infection.

Results

1q42 Break Site Mapping

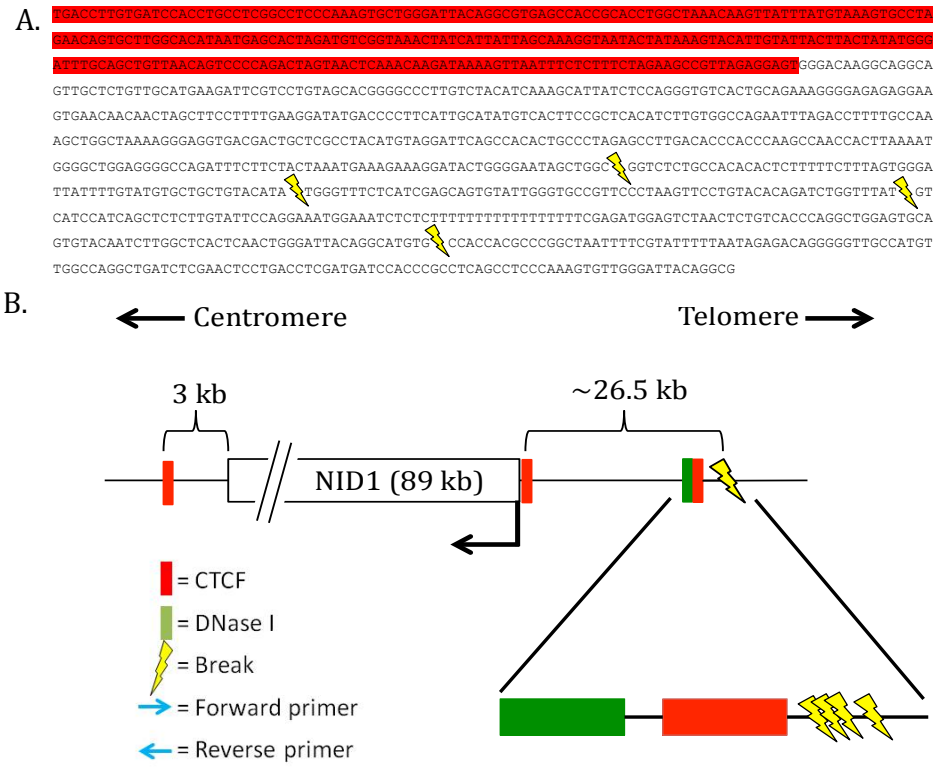

Figure 16: Mapped location of DNA breaks on 1q42 induced by HCMV infection (A) Repeated LMPCR revealed 4 breaks within a ~350 base pair region. Red highlighted text indicates a CTCF binding region (with consensus within). Lightning bolts indicate mapped HCMV-induced breaks. (B) The mapped breaks with respect to the NID1 gene, as well as CTCF binding sites and DNAse hypersensitivity sites.

Repeated LMPCR amplification and sequencing of the 1q42 break site region revealed four different breaks within a ~350 base pair region (Figure 16). The locations of the breaks are just 3' to a CTCF binding site. It appears the breaks are not occurring at the

same location each time, suggesting the DNA may be broken by protein interactions at a fragile site and not by a specific cleavage event.

1q42 Break Site Deep Sequencing

In the first iteration of this experiment, we used three sets of cells (mock infected HFFs, HCMV infected HFFs, and long term infected neurons). There were four different time points for the mock and infected HFFs and two time points for the mock and infected long term infected neurons. Two primer pairs were used to amplify each one, making a total of 24 total samples. Each sample contained ~5.5 x 10^5 cell equivalents. The predicted number of reads we would receive totaled ~2.125 x 10^6 reads. The number of reads per sample totaled 0.59 reads per cell and 0.295 reads per chromosome (Figure 17). Using a large number of samples and cell equivalents in the deep sequencing reaction was problematic because we were not able to get enough reads to cover all the potential sequences in the reaction. Because only repaired DNA can be sequenced, we

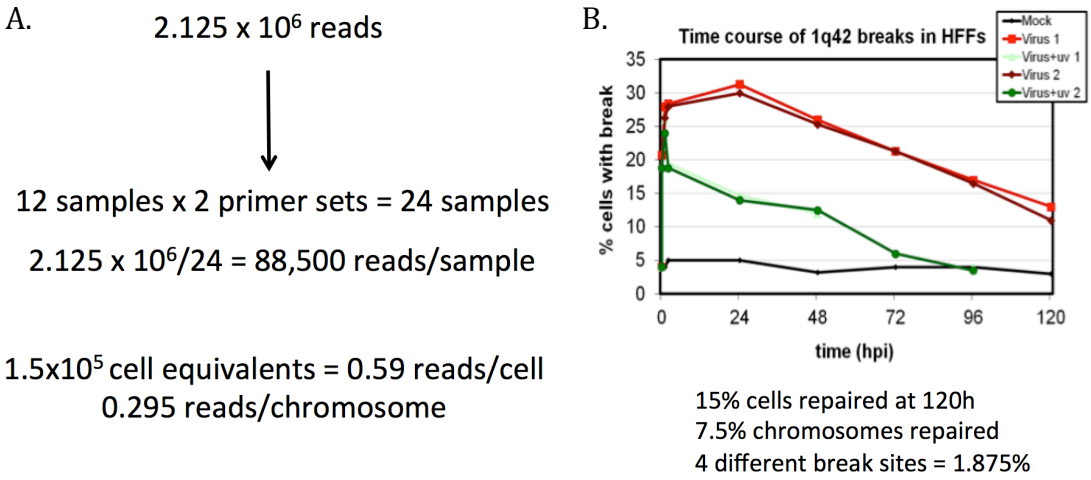

Figure 17: (A) Calculation of reads per chromosome in experiment one. (B) Breakage frequency of infected fibroblasts at the 1q42 break site. See text for details.

expected the sequence of early time points to very closely resemble the mock-infected samples because no repair has occurred. We further expected later time points to have a much higher frequency of sequence changes because they have had time to repair the breaks. At late time points, repaired DNA could be a low percentage of the population (7.5% of chromosomes repaired at 120h). A large number of reads per cell was necessary in order to amplify the signal of aberrant sequences that are a small proportion of the population.

The maximal length of PCR amplicons for deep sequencing is ~550 base pairs because the Miseq is designed to read ~300 bp from both directions, providing ~25-50 bp for overlap in the middle. In the first experiment, we designed two primer pairs, BB3F/BB5R and BB4F/BB5R (Figure 18). The resulting PCR products would be 550 base pairs and 350 base pairs, respectively. Although our amplicons were within the

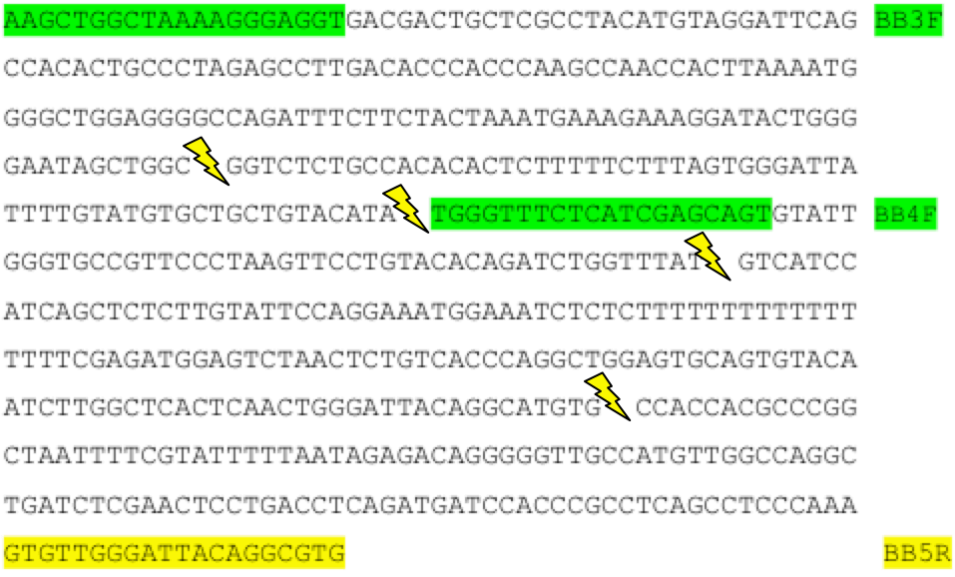

Figure 18: The sizes of PCR amplicons in the first experiment were 550 base pairs (BB3F/BB5R) and 350 base pairs (BB4F/BB5R).

suggested max length, the quality of our reads from either end of the primer pairs decreased significantly after ~100-200 base pairs. We decided to design new primers to amplify much smaller sections of the break site as well as amplifying overlapping regions of DNA for the second experiment.

In the second experiment, we used fewer samples (3 total), a smaller number of cell equivalents (1000 cells), and created smaller amplicons (3 overlapping) in order to increase the read quality (Figure 19). The resulting mock 24 hpi reads were compared with virus 24 and 120 hpi samples using two different variant caller programs, Mutect and Varscan2 (Cibulskis et al. 2013 and Koboldt et al. 2012). Mutect was originally developed to identify somatic point mutations in next generation sequencing data of cancer genomes. It looks at reads of "normal" tissue and compares them to reads of

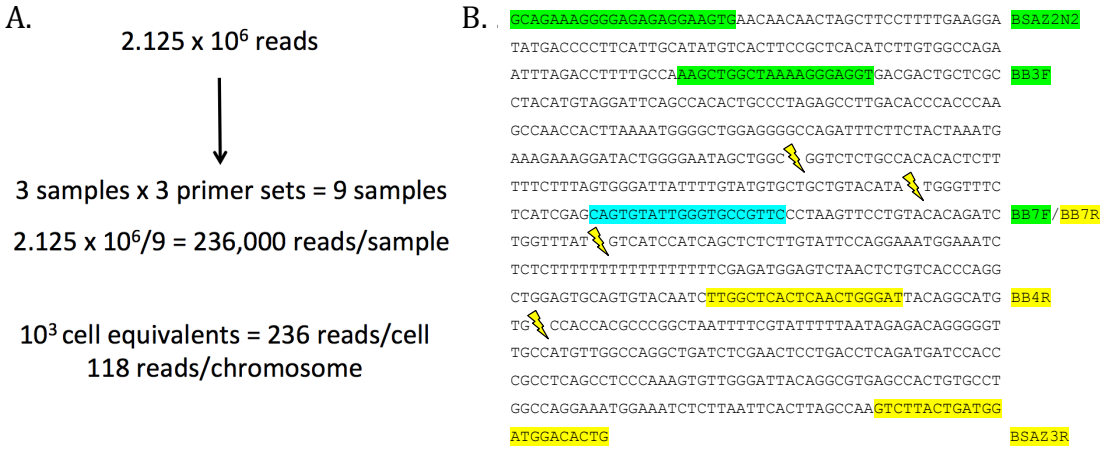

Figure 19: (A) Calculation of reads per chromosome in experiment two. (B) In the second experiment, we used three primer pairs to make amplicons that are less than 400 bp. See text for details.

"tumor" tissue and identifies point mutations. For the Mutect analysis, the mock infected reads were designated as "normal" and the HCMV infected reads were designated as "tumor." Varscan2 was originally developed to detect variants in cancer

genomes. Varscan2 compares “normal” and “tumor” tissue and identifies insertions and deletions. As with the Mutect analysis, we designated mock infected reads as “normal” and HCMV infected reads as “tumor.” The output from both of these variant callers shows there are sequence differences between mock and virus-infected cells, but analysis is still ongoing.

HCMV and Break Site Sequence Comparison

To predict how a viral protein may be interacting with the DNA at each break site, we performed sequence comparisons with the HCMV genome. It is possible that a viral protein could be binding to chromosome one due to sequence similarities with the HCMV genome. Resulting BLAST data shows that around the mapped 1q42 and 1q23 break sites and CTCF binding sites, there is a clustering of homology to the HCMV genome. There is greater HCMV sequence homology to break site regions 1q42 than a similar site that is not broken during infection. The similar site is located at 1p31 (the short arm of chromosome 1) and it contains a CTCF binding region on the short arm of chromosome one (Figure 20). Additionally, there is gre ater sequence homology to the 1q23 break site region than a non-broken site at 12q23, which also contains a CTCF binding site (Figure 21). We also compared the genome of other herpesviruses (EBV and HSV-1) that don’t cause DNA damage during infection. EBV has very little sequence homology to the 1q42 and 1q23 break sites (Figure 22). HSV-1 has very little sequence homology to the 1q42 break site, but quite a bit to the 1q23 break site (Figure 23). When we compared the regions of homology of HSV-1 and HCMV at 1q23, we found a large majority of the sites fall in the same location on 1q23 (Figure 24). More analysis

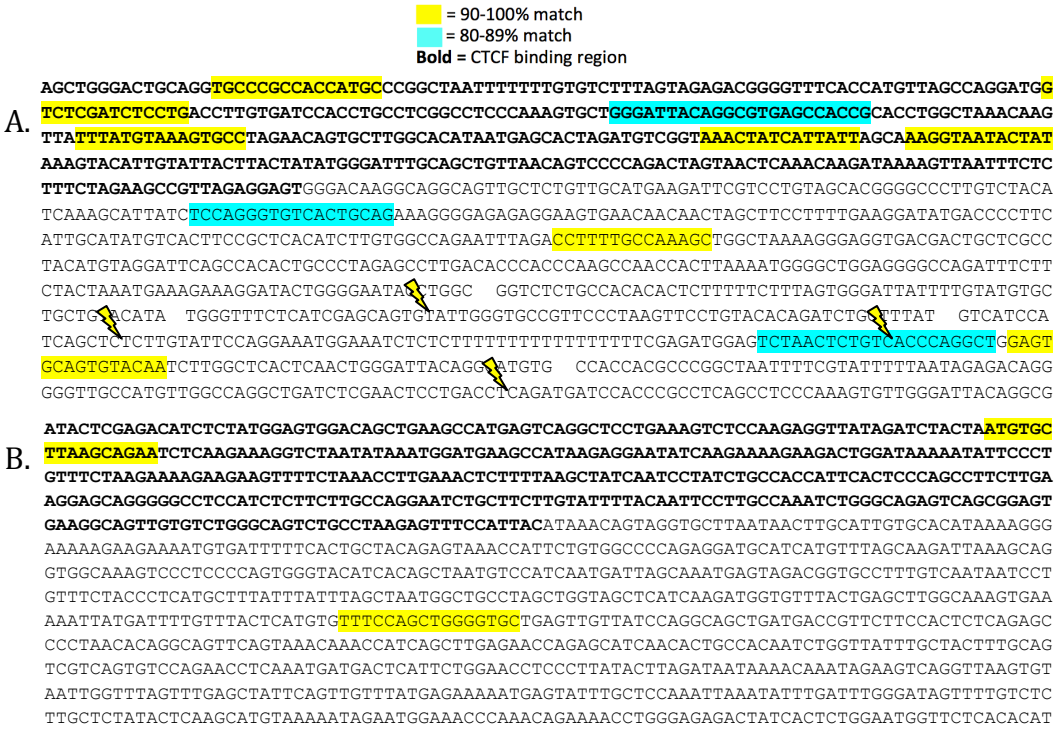

Figure 20: There is greater HCMV homology to break site region 1q42 than a non-broken site at 1p31. (A) Break site region 1q42 has clustered sequence homology to HCMV. (B) A similar site at 1p31 that is not broken upon infection shows very little sequence homology.

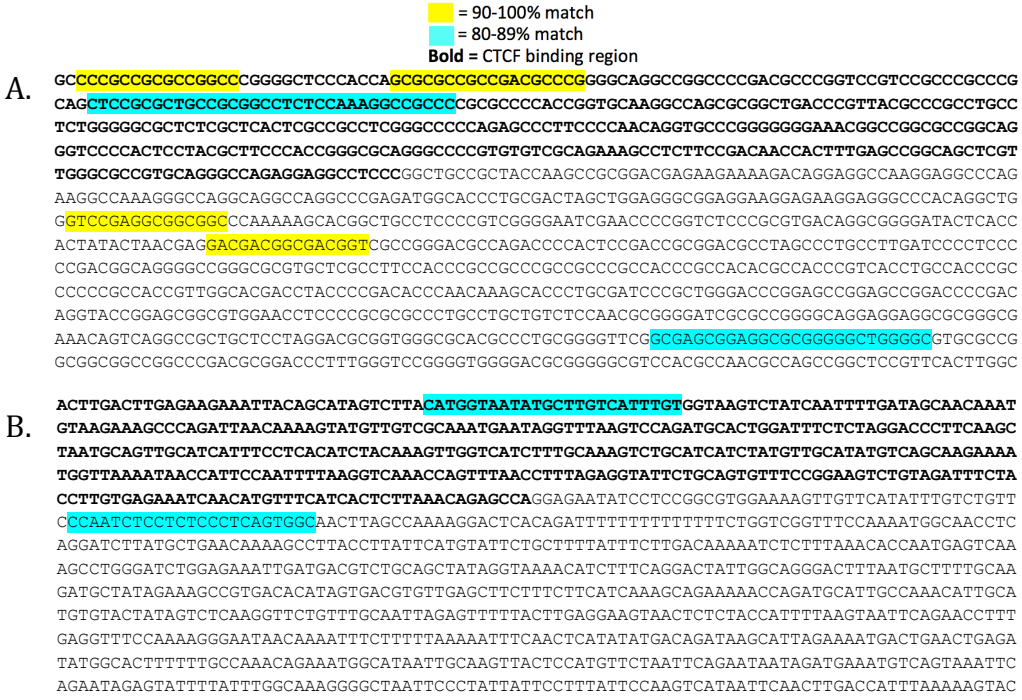

Figure 21: There is greater HCMV sequence homology to the 1q23 break site region than a non-broken site at 12q23. (A) Break site region 1q23 has clustered sequence homology to HCMV near the CTCF binding site. (B) A similar site with a CTCF binding region at 12q23 that is not broken upon infection shows very little sequence homology.

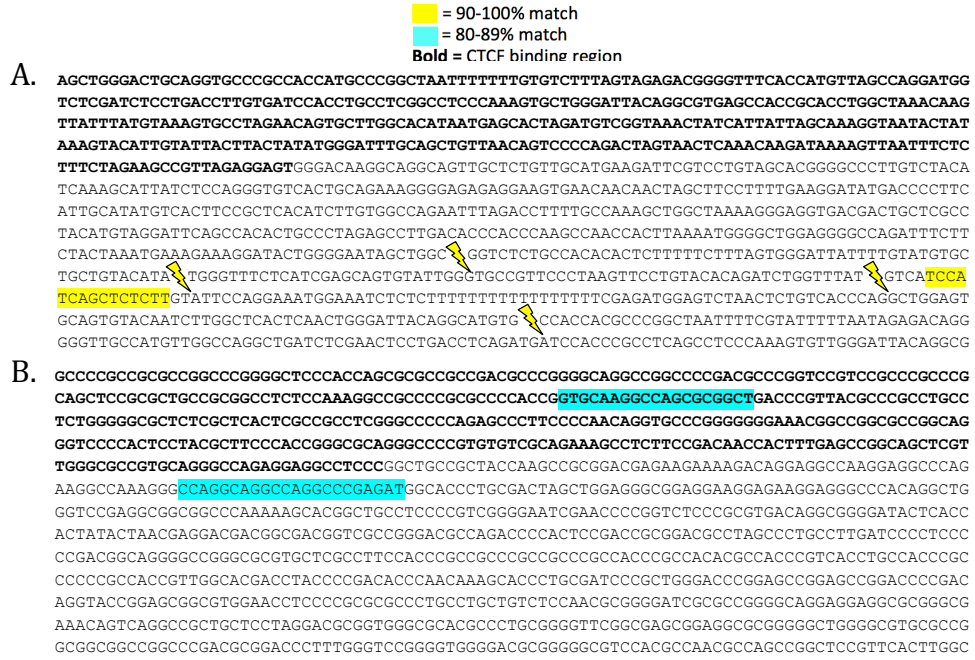

Figure 22: Sequence comparison of the EBV genome to the chromosome one break sites. (A) Lightning bolts indicate mapped HCMV induced breaks at 1q42. There is very little sequence homology to EBV, which doesn't cause DNA damage upon infection. (B) Similarly, there is very little sequence homology to EBV at the 1q23 break site.

Figure 23: Sequence comparison of the HSV-1 genome to the chromosome one break sites. (A) Lightning bolts indicate mapped HCMV induced breaks at 1q42. There is very little sequence homology to HSV-1, which doesn't cause DNA damage upon infection. (B) Interestingly, there is a larger amount of HSV-1 sequence similarity at the 1q23 break site.

will need to be done to compare the regions of homology on the HSV-1 and HCMV genomes to determine if homologous genes have similarity with 1q23.

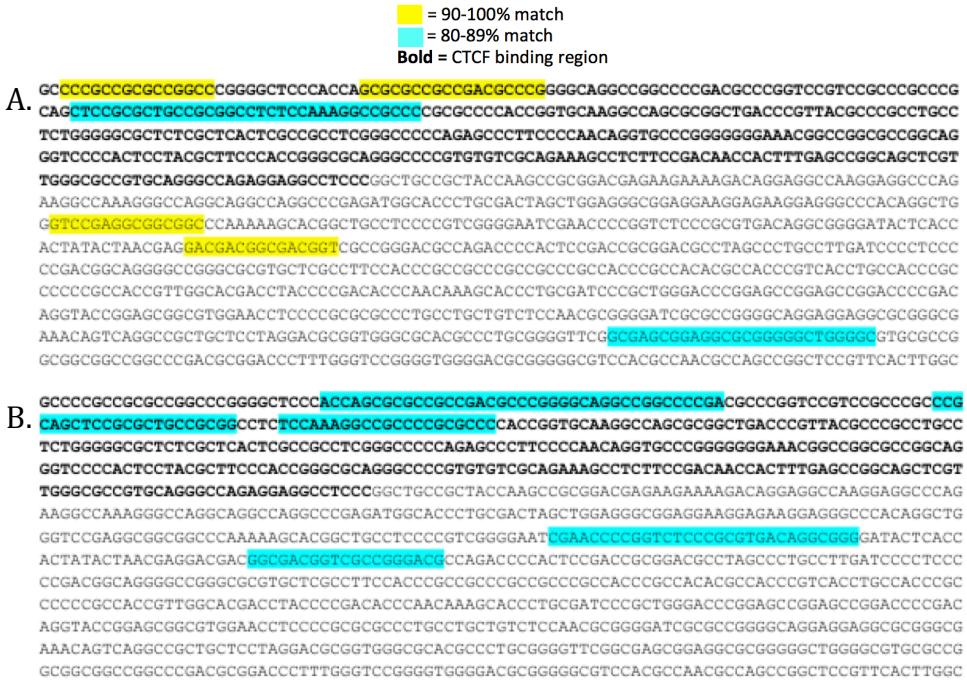

Figure 24: Sequence homology of HCMV (A) and HSV-1 (B) at the 1q23 break site. A large majority of the sites fall within the same regions along 1q23. More analysis will need to be done to determine if the viral genes that have similarity to this regions are homologs.

Discussion and Conclusions

The DNA damage project was focused on identifying the specific location of the breaks at the 1q42 break site, investigating possible incorrect DNA repair at 1q42, and determining how a viral protein may be interacting with the DNA at the break sites. We used LM-PCR to map the break site region at 1q42 and found four different break sites within a ~350 bp region. This suggests that the DNA is not specifically cleaved, but is perhaps damaged by the interaction of a viral protein either directly with the DNA or with cellular proteins at a fragile site. The break sites lie just 3' to a CTCF binding site.

The transcriptional down-regulation of break site genes NID1 and MPZ suggests that the DNA damage could be interrupting an enhancer for these genes. At 24 hpi, 30% of infected HFFs have the break at 1q42. This declines to 15% over a 120 h time course, suggesting the breaks are being repaired. Previous work in our lab has shown that HCMV interacts with host DNA damage machinery. This led us to hypothesize that the breaks introduced during infection are not properly repaired. Improper repair at these sites could lead to sequence changes such as insertions/deletions and could prevent an activator protein from properly binding. There appears to be differences in the mock and viral sequences, but the data is still being analyzed.

To predict how a viral protein may be interacting with the DNA at the chromosome one break sites, we compared their sequences to the genome sequence of HCMV. A high degree of sequence similarity to HCMV was present at both the 1q42 and 1q23 break sites. The similarity was clustered around the CTCF binding sites, as well as the mapped break sites at 1q42. A lower degree of similarity to HCMV was present at other regions of the genome that also contained a CTCF binding region. This suggests that a viral protein may be binding to the break sites by mistake during infection. Herpesviruses (EBV and HSV-1) that don't cause DNA damage during infection also had a lower degree of sequence similarity at our break site regions.

Breaks occur upon infection with transcriptionally inactive virus, meaning the viral protein responsible for the DNA damage is not *de novo* synthesized and is brought into the cell with the virus. We suspect tegument protein pp71 is responsible for HCMV

induced DNA damage at the 1q42 and 1q23 break sites. pp71 is a tegument protein that transactivates the MIEP and causes IE genes to be expressed. Adjacent to the breaks at 1q42, there is a CTCF binding site. CTCF negatively regulates major immediate early (MIE) gene expression during HCMV infection. It binds directly with the DNA in the first intron of the MIE gene and blocks interaction of RNA polymerase II function during the early stages of viral transcription. Recent work in our lab has shown that transfection of pp71 alone causes breaks on chromosome one. Additionally, we have seen CTCF bound to the 1q42 break site after infection. It is possible that CTCF binds to the MIE gene to repress transcription and pp71 attempts to remove it in order to activate transcription. There is a high degree of similarity between HCMV and the chromosome one break site regions. Because of this high degree of similarity, it is possible that pp71 is binding to the break site regions by mistake and attempting to remove CTCF that is bound there. This could cause torsion on the DNA, resulting in damage.

CHAPTER 3: CEREBRAL ORGANOIDS AS A MODEL FOR CONGENITAL HCMV INFECTION

Introduction

Cerebral Organoids are a Clinically Relevant Model

Fetuses that are infected with HCMV during the first half of gestation develop more serious neurological defects (Pass et al. 2005). To study this, we used cerebral organoids, a three-dimensional brain development model that utilizes pluripotent stem cell growth and development. We used induced pluripotent stem cells (iPSCs) as a starting material to culture the organoids. iPSCs are somatic cells that have pluripotency genes OCT4, KLF4, SOX2, and c-Myc introduced via a viral vector (Takahashi and Yamanaka 2006). Our cells are derived from fibroblasts and reprogramming genes were introduced via a lentiviral vector. Cerebral organoids were initially developed to study microcephaly in patient-derived iPSCs (Lancaster et al. 2013) and have recently been used for Zika virus studies (Dang et al. 2016 and Cugola et al 2016). This new technology also has potential to help us understand infectious diseases of the central nervous system, such as congenitally acquired HCMV. Previous studies (D'Aiuto et al. 2012, Nakamura et al. 2013) have cultured iPSCs as an adherent monolayer (2D cell culture). Infected iPSCs have been differentiated into various cell types such as neurons and glia via the 2D culture system. This culture method is useful for some aspects of HCMV study, but does not mimic the architecture and environment of the brain. In order to keep the cells adherent, they need to be cultured on an artificial matrix that is high in NID1. This makes it impossible to study the organization of NID1

and how it is impacted by infection. Cerebral organoids are a valuable tool to see how structure formation, cellular proteins (such as NID1), and different cell types are affected by HCMV infection. The successful development of cerebral organoids as a novel method of modeling HCMV infection would be much more clinically relevant than 2D culture of neurons or glia alone. They can help us see how HCMV affects brain development at very early time points that can't be seen with clinical samples or 2D cell culture.

The Role of NID1 and MPZ During HCMV Infection

Preliminary data shows there is transcriptional down-regulation of both NID1 (at 1q42) and MPZ (at 1q23) during infection, while other adjacent genes appear unregulated. Clinical temporal bones stained for nidogen-1 and MPZ also show down regulation in infected samples. The down regulation of both NID1 and MPZ in clinical samples infected with HCMV could contribute to sensorineural hearing loss that is common in infected infants.

Although we are interested in studying MPZ, we cannot use cerebral organoids to do so. MPZ is made by Schwann cells, which are exclusively located in the peripheral nervous system and can not be modeled by cerebral organoids Further study into the role of MPZ is outside the scope of this study, but future studies with infected Schwann cells are planned.

Materials and Methods

Cerebral Organoid Culture and Infection

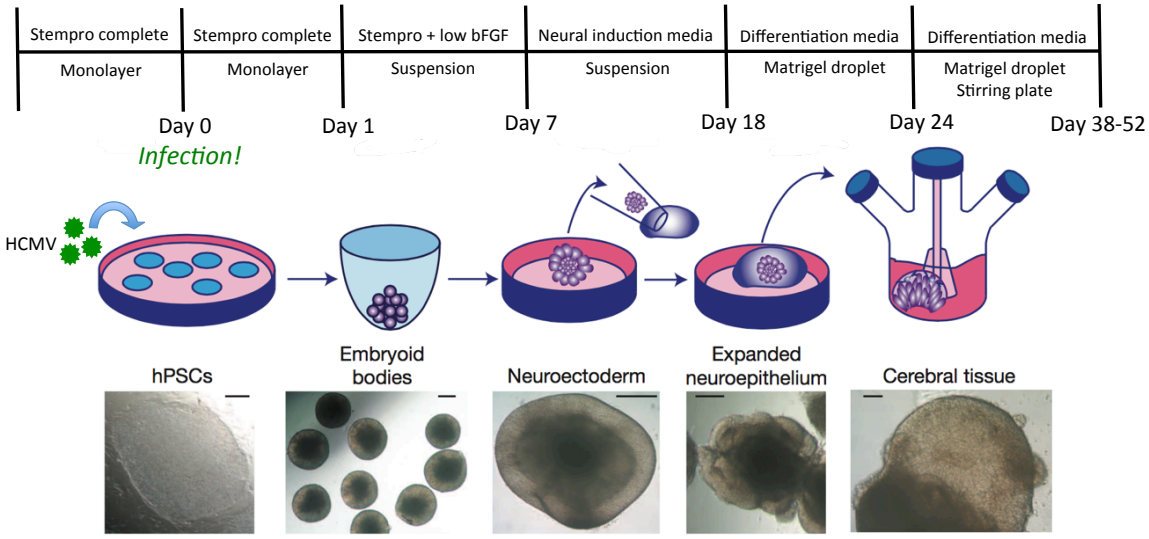

Figure 25: Timeline of cerebral organoid culture from iPSCs to fully formed organoid See text for details. Reprinted with permission from Macmillan Publishers Ltd: Nature (Lancaster et al.), copyright 2013.

Induced pluripotent stem cells (iPSCs) are used as a starting material to culture cerebral organoids (Figure 25). IPSCs are somatic cells that have pluripotency genes OCT4, KLF4, SOX2, and c-Myc introduced via a viral vector (Takahashi and Yamanaka 2006). We have slightly modified the originally established organoid culture protocol (Lancaster et al. 2013). Stem cells are maintained in culture as a monolayer until they are confluent in stempro complete media containing DMEM F-12 with Glutamax (Gibco), 1.8% BSA (Gibco), 55 µM 2-Mercaptoethanol, 2% penicillin-streptomycin (Corning, 20 ng/mL bFGF (Prospec), and Stempro hESC supplement (Gibco). While the cells are still in a monolayer, they are infected with HCMV at an MOI of 5. 24 hours later, the cells are stimulated to form neural spheres by placing them into neural induction media containing DMEM F-12 (Gibco), 1% N2 supplement (Gibco), 1% Glutamax

(Gibco), 1% MEM-NEAA (Gibco), and 1% penicillin-streptomycin (Gibco). At this time, they will continue on their differentiation pathway to become NPCs. When the spheres have smooth and transparent edges (about a week later), they are embedded into a matrigel (Corning) droplet in order to provide a "scaffold" for the organoids to grow into. They are transferred into differentiation media containing a 1:1 mixture of DMEM F-12 (Gibco) and Neurobasal medium (Gibco) with 0.5% N2 supplement (Gibco), 20 μM 2-Mercaptoethanol, 1% Glutamax (Gibco), 0.5% MEM-NEAA (Gibco), 1% penicillin-streptomycin (Gibco), and 0.5% B27 without retinoic acid (Gibco) five days after embedding. After an additional five days (10 days after embedding), B27 with retinoic acid (Gibco) is added instead of B27 without retinoic acid into the differentiation medium. At this time, the organoids are also put on to an orbital shaker to circulate the media. Cerebral organoids are harvested 38-52 days after placement into neural induction media.

Organoid Fixation, Embedding, and Sectioning

Organoids were fixed in 4% para-fomaldehyde diluted in PBS at 4°C for 20 minutes and washed with PBS 3 times at room temperature. They were then submerged in 30% sucrose diluted in PBS at 4°C until they sank to the bottom of their container. For long term storage, organoids were flash frozen in 30% sucrose and stored at -80°C. After sinking in sucrose, the organoids were submerged in a 1:1 mixture of OCT and 30% sucrose and placed on an orbital shaker at room temperature for 30 minutes. Organoids were then embedded in pure OCT, flash frozen, serially sectioned with a cryotome into

14 μm sections, and mounted on positively charged microscope slides. Sections were stored at -20°C until stained.

iPSC Coverslip Culture

IPSCs were seeded in parallel on to matrigel-coated coverslips and differentiated in a monolayer using the cerebral organoid protocol listed above.

Hematoxylin and Eosin Staining

The first, middle, and last slides of serially sectioned organoids were thawed at room temperature and soaked in 1X PBS for 1 minute. The slides were placed into hematoxylin for 5 minutes, rinsed with water, soaked in 1X PBS for 2 minutes, placed in eosin for 5 minutes, and decolorized in 80% ethanol for 1 minute. Tissues were dehydrated through two 2 min washes in 100% ethanol before soaking in two washes of histoclear two times for 2 minutes each and then mounted with permount. Analysis and imaging of H&E stained organoids was performed on a Nikon Eclipse E800 microscope equipped with a Nikon DS-Ri1 camera and Nikon Elements software.

Measurement of Sectioned Organoids

The largest tissue section of each organoid was picked for measurement. The sections were imaged at 10X and the longest and shortest portions were measured using Nikon Elements Software. The rough volume of the organoids was calculated using these measurements.

Sectioned Organoid Immunofluorescence

Serially sectioned organoids mounted on microscope slides were thawed at room temperature and the slide was divided horizontally with a pap pen. The slides were soaked in 1X PBS for 5 minutes and then permeabilized with 1% Triton X-100 for 5 minutes at room temperature in PBS. Slides were blocked with 30% FBS in blocking solution (PBS with 1% BSA and 0.01% Tween 20) for 20 minutes at room temperature in a humidity chamber and then treated with specific primary antibodies diluted in blocking solution for 90 minutes. The slides were then washed three times in 1X PBS and treated with specific secondary antibodies and Hoechst dye diluted in blocking solution for another 90 minutes. The slides are then rinsed extensively with 1X PBS and mounted with 70% glycerol. For epifluorescent analysis, organoids were examined and photographed on a Nikon Eclipse E800 fluorescence microscope equipped with a Nikon DS-Ri1 camera and Nikon Elements software. For confocal analysis, organoids were photographed on a Nikon Andor Spinning Disk confocal microscope using a Xyla sCMOS camera. Image analysis was done on Imaris software.

iPSC Coverslip Immunofluorescence

Plates were loaded with coverslips, cells were seeded, grown, and infected at an MOI of 5 as described above. The coverslips were harvested at given time points post infection, rinsed with 1X PBS, and fixed in 3% formaldehyde diluted in 12.5% sucrose diluted in PBS at 37°C for 5 minutes. The cells were then washed three times with 1X PBS, permeabilized with 1% triton in PBS for 5 minutes at room temperature, and quickly rinsed again with 1X PBS. Coverslips were blocked with 30% FBS in a blocking solution

(PBS with 1% BSA and 0.01% Tween 20) for 30 minutes at room temperature in a humidity chamber. The cells were rinsed with 1X PBS and treated with specific primary antibodies diluted in blocking solution for 30 minutes. The coverslips were then washed three times with 1X PBS and treated with specific secondary antibodies diluted in blocking solution for 10 minutes. The coverslips are then rinsed again with 1X PBS and mounted in 70% glycerol. Nuclei were counterstained with Hoechst. Epifluorescent analysis was done as described above.

Whole Organoid Immunofluorescence Confocal Imaging

Organoids were fixed as described above, rinsed extensively with 1X PBS, and blocked in blocking solution (PBS with 1% BSA and 0.4% Triton X-100) overnight at 4°C. The organoids were treated with specific primary antibodies (anti-beta tubulin III, nidogen-1, and IE1) diluted in blocking solution overnight at room temperature and washed 3 times with 1X PBS on an orbital shaker. They were then treated with specific secondary antibodies diluted in blocking solution overnight at room temperature and washed three with 1X PBS. Confocal imaging was done with an Olympus Fluoview upright microscope system with z-steps of 25 μm. Images were taken of a whole organoid suspended in 1X PBS inside a small glass cloning ring at 10X. We were not able to image the entire organoid in one field of view, so we imaged small portions of the organoid at a time. Images were taken in a grid around the entirety of the tissue. Whole z stacks were projected on to one plane and stitched together to form an image of the entire organoid. During stitching, landmarks around the tissue were used to aid in piecing together the entire organoid.

Antibodies

Primary antibodies: mouse anti-MAP2 (Sigma), mouse anti-Beta tubulin III (Sigma-Aldrich), rabbit anti-PAX6 (Gift from Phil Pellett), mouse anti-Nestin (Chemicon International), mouse anti-UL44 (Virusys), mouse anti-IE1 (Gift from Bill Britt), rat anti-Nidogen 1 (Chemicon International), mouse anti-gB (Virusys), mouse anti- pp65 (Virusys) and mouse anti-pp71 (Gift from Rob Kalejta).

Secondary antibodies: Alexa Fluor 488 conjugated goat anti-mouse IgG1 and IgG2a (Molecular Probes). TRITC conjugated goat anti-mouse IgG2a (Southern Biotech)and TRITC conjugated donkey anti-rabbit (Jackson ImmunoResearch Laboratories). Rhodamine conjugated donkey anti-rat (Jackson ImmunoResearch Laboratories).

Whole Organoid Auto-Fluorescence Confocal Imaging

Whole organoids were fixed as described above and suspended in 1X PBS inside a small glass cloning ring. The auto-fluorescence of paraformaldehyde was utilized to image possible structural elements within whole organoids. Auto-fluorescence images were taken with the 488 nm laser at 10X with 25 μm z-steps using an Olympus Fluoview upright microscope system. We were not able to image an entire organoid in one field, so we imaged small portions of the organoid at a time. Images were taken in a grid around the entirety of the tissue. Whole z stacks were collapsed and stitched together to form an image of the entire organoid. During stitching, landmarks around the tissue were used to aid in piecing together the entire organoid.

Whole Organoid Measurement

Whole organoids were fixed as described above, suspended in 1X PBS and imaged on a Leica MZ16 stereoscope. A hemacytometer was imaged alongside the organoids in order to generate a scale for measurement. Using the whole organoid images, the diameter was measured at the largest and smallest portion of the organoid. Measurements were made in pixels on Nikon Elements Software and converted to mm based on the number of pixels in one mm on the hemacytometer. Because we were unable to measure the depth of the organoids, the smaller diameter measurement was used in its place. The rough volume of the organoids was calculated with the formula $4/3\pi(\text{long radius})(\text{short radius})^2$ using these measurements.

Results

Susceptibility of iPSCs to HCMV Infection Under the Organoid Differentiation Protocol

Induced pluripotent stem cells, the cells used for cerebral organoid differentiation, are susceptible to HCMV infection, but they are not permissive. This means the virus can bind and enter the cells, but there are no *de novo* viral antigens expressed and the virus does not replicate. Interestingly, neural progenitor cells (NPCs) derived from iPSCs are fully permissive to HCMV infection (D'Aiuto et al. 2012). This suggests that HCMV infection in iPSCs enters latency and is reactivated as the cells differentiate into NPCs. Neonatal NPCs, neurons, and glia derived from NPCs are also fully permissive to HCMV infection (Luo et al. 2008). Infected neonatal NPCs undergo premature and abnormal

differentiation. Multipotency genes and neural identity genes are down regulated in these infected NPCs (Luo et al. 2010). Differentiation of iPSCs using the cerebral organoid model is very different than neuron differentiation. It was unclear to us whether the organoids would develop a robust, productive infection under these differentiation conditions.

In order to determine whether iPSCs became fully susceptible to HCMV infection under the cerebral organoid differentiation protocol, we infected induced pluripotent stem cells attached to glass coverslips in a monolayer. 24 hours later, we began differentiation of these cells using the cerebral organoid protocol. Coverslips were harvested and stained using immunofluorescence for viral tegument protein pp65 and immediate early protein IE1 to look for viral entry into the nucleus and *de novo* protein synthesis, respectively. At 24 hpi, approximately 15% of the cells stained positive for pp65 and negative for IE1. This indicates the virus entered the cells and trafficked to

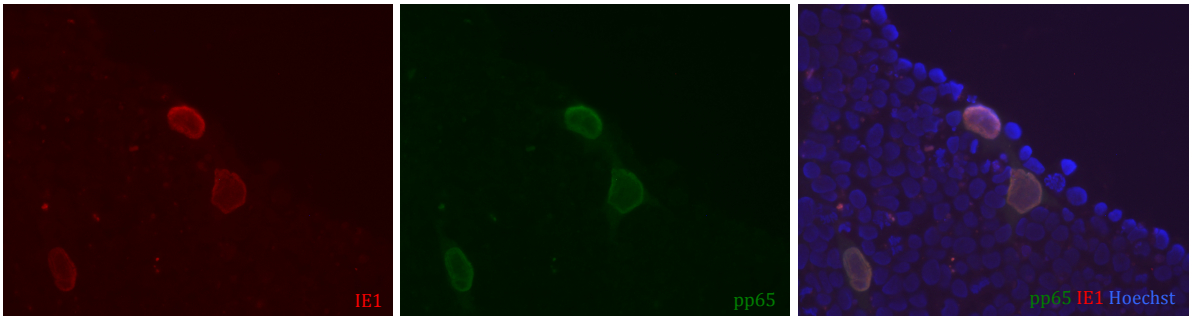

Figure 26: Viral antigen staining in HCMV infected iPSCs. Infected SC30i cells express both IE1 (left) and pp65 (middle) at 6 DPI, indicating *de novo* protein synthesis has begun and the cells are indeed to permissive to HCMV infection.

the nucleus, but no new viral protein was being expressed. At 48h, the cells stained negative for both pp65 and IE1, indicating the input pp65 protein had been degraded and there had been no new protein synthesis. The cells remained negative for both

pp65 and IE1 until 6 dpi, when a proportion of them became positive for both (Figure 26). This indicated *de novo* protein synthesis had begun and the cells were indeed permissive to HCMV infection by 6 dpi.

Structural Characterization of Cerebral Organoids

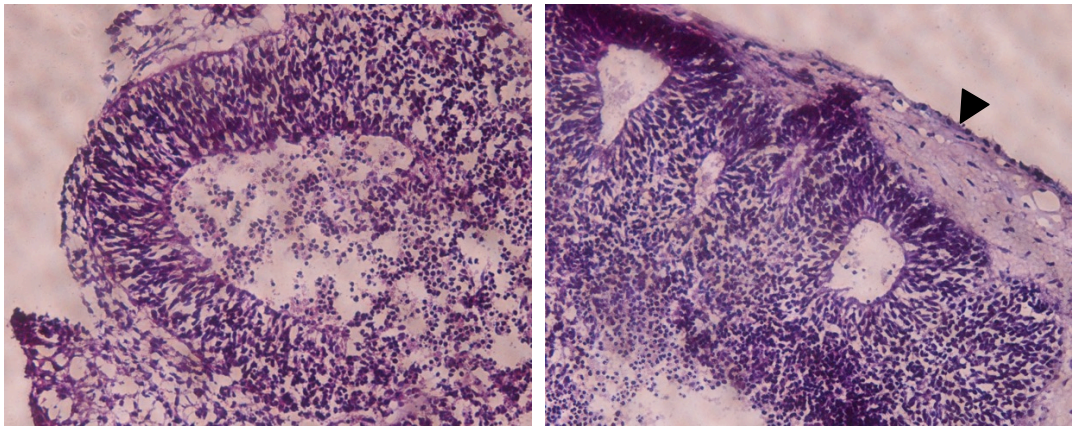

Figure 27: Hematoxylin and eosin staining shows cerebal structures organized into circular and arch shapes as well as supportive structures (arrowhead) that appear to surround cerebral structures and providing an extracellular matrix.

The researchers who first described cerebral organoid culture showed structures reminiscent of cerebral cortex that developed internally (Lancaster et al. 2013). Characterization of cell types and protein markers revealed neural progenitor populations (stained with PAX6) within cerebral structures and neural markers (beta tubulin III, MAP2, and nestin) throughout the organoids (Lancaster et al. 2013). To characterize the cerebral organoids, we first stained with hematoxylin and eosin (H&E) to observe internal structures. Next, we used immunofluorescence to determine the presence and organization of cellular proteins. H&E staining showed that there were two distinct structures found within the organoids, cerebral-like structures and supportive structures (Figure 27). The cellular arrangement of cerebral structures is

highly organized into circular and arch shapes. Supportive structures are much less cell dense and seem to be surrounding cerebral structures, perhaps providing an extracellular matrix. Although supportive structures were seen in previously described organoids, attention was not drawn to their existence. Immunofluorescence shows the presence of NPC markers (PAX6) within cerebral structures and neuronal markers (beta tubulin III) around the outer rim, the inner rim, and extending between the two (Figure 28). This observed organization of NPCs and terminally differentiated neurons resembles the sub-ventricular zone in the developing fetal brain. The cellular organization and protein markers of cerebral structures we observed are comparable to those described previously (Lancaster et al. 2013).

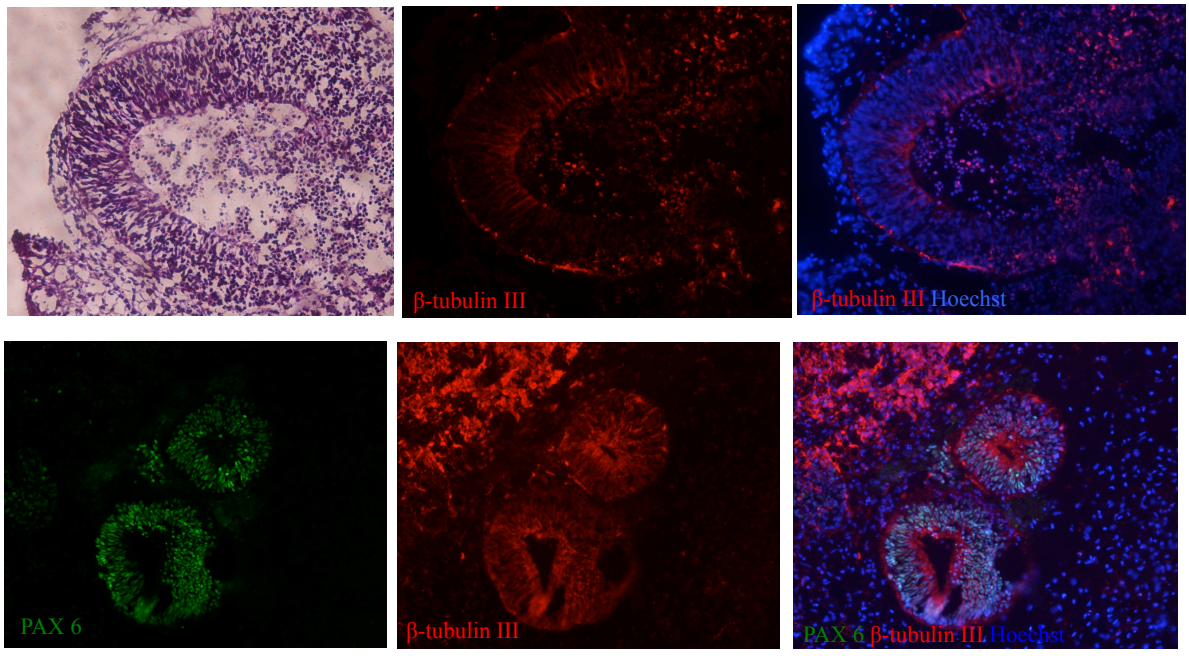

Figure 28: Cerebral structures present in organoids are comparable to those previously described (Lancaster et al. 2013). Neuron marker beta tubulin III stains around the outer and inner rim of cerebral structures and spans the gap in between. PAX6 staining is present in the interior of cerebral structures and beta tubulin III stains around the rims of these structures, resembling the fetal sub-ventricular zone.

Organoid Measurement

The first set of organoids we cultured varied widely in the number of internal cerebral structures and in size, regardless of infection status. The original culture protocol (Lancaster et al. 2013) did not include a guideline regarding specific developmental milestones that "successful" organoids should reach. A more detailed protocol paper was released that contained a very detailed record of developmental milestones that should be reached (Lancaster and Knoblich 2014). All of our initial organoids were cultured until 38 or 52 days, regardless of their developmental level. The approximate volume of these organoids varied widely, with standard deviations ranging from 258.85- 1158.68 mm^3 (Figure 29). Subsequent sets of organoids were "culled" based on the guidelines provided in the updated protocol paper. These organoids were divided into two groups, those with small neuroepithelial buds adjacent to the developing neuroectoderm during the embryoid body stage, and those without. The resulting organoids were much more consistent in their size and apparent developmental stage, with standard deviations ranging from 49.18-122.12 mm^3 (Figure 30).

Because microcephaly is a common defect in congenital HCMV infection, we wanted to compare the overall size of mock and HCMV-infected brains. The organoids that were culled based on the new protocol were imaged whole using a stereoscope (see Figure 35) and the images were used to calculate approximate volumes. Based on these

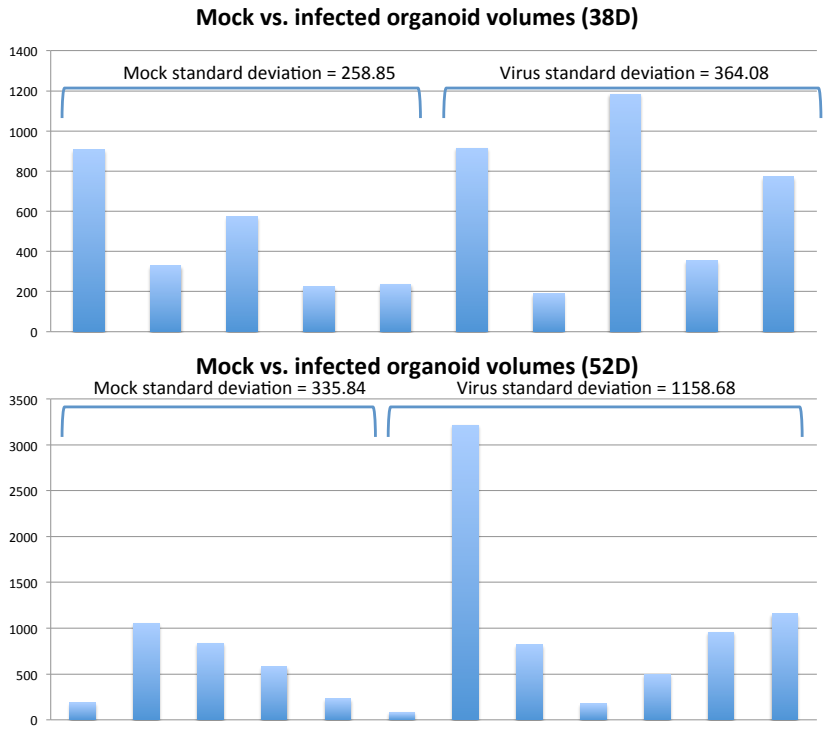

Figure 29: Approximate volume of cerebral organoids that were not culled based on developmental milestones. The volume of both 38 and 52-day-old organoids varied widely, with standard deviations ranging from 258.85-1158.68 mm^3.

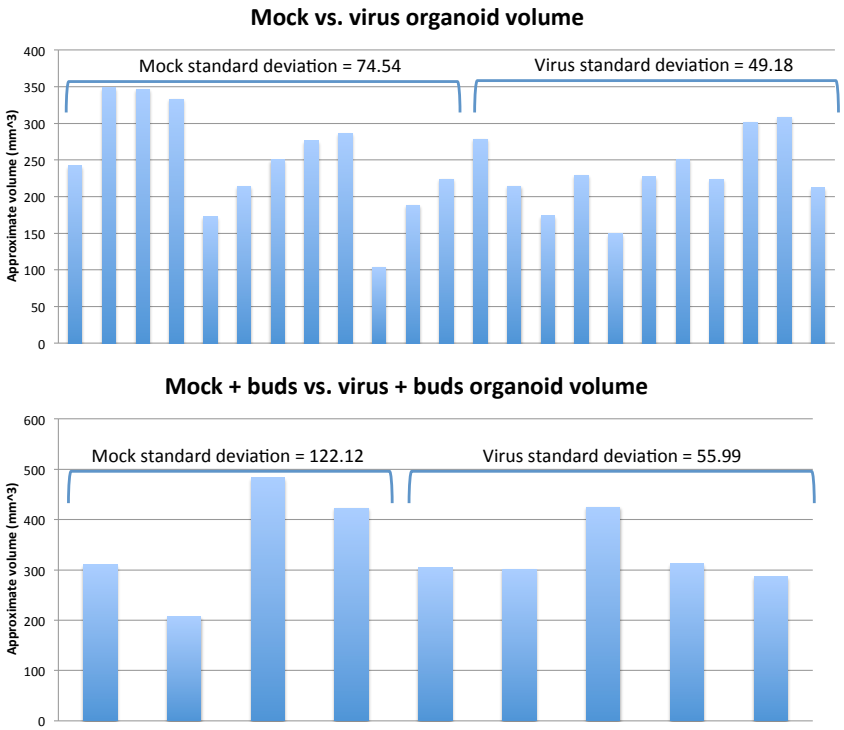

Figure 30: Approximate volume of cerebral organoids that were culled based on developmental milestones. The volumes of both normal organoids and organoids with buds were much more uniform, with standard deviations ranging from 49.18-122.12 mm^3.

calculations, we do not see a statistically significant difference in overall size between mock and HCMV infected organoids (Figure 31).

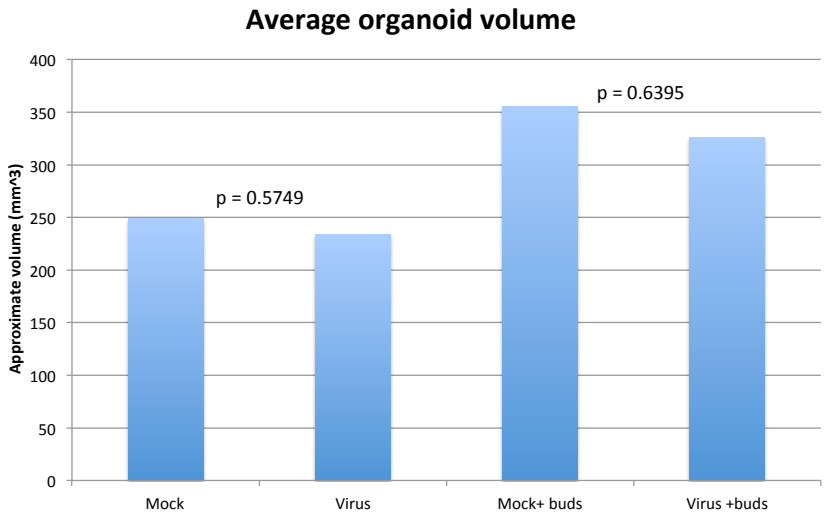

Figure 31: Average approximate volume of set 4 organoids. Resulting organoids cultured using the updated protocol are more uniform in size. There is no significant difference in overall size between mock and HCMV infected organoids.

HCMV Infection Status of Infected Organoids

We stained organoids using immunofluorescence to determine if they could be productively infected with HCMV. To determine if the organoids were supporting a full cycle of infection, we stained for three different classes of viral proteins, including IE1 (an immediate early protein), UL44 (an early protein), and gB (a late protein). Presence of IE, E, and L proteins indicated a full cycle of infection. Organoids harvested at both 38 and 52 days post infection showed viral antigen positivity in focal regions and stained positive for all three classes of viral proteins (Figure 32a). The focal nature of the viral antigen positivity made it difficult to determine the exact localization of staining with

epifluorescence. Confocal microscopy confirmed IE and E viral antigen positivity was localized to the nucleus, as would be expected (Figure 32b).

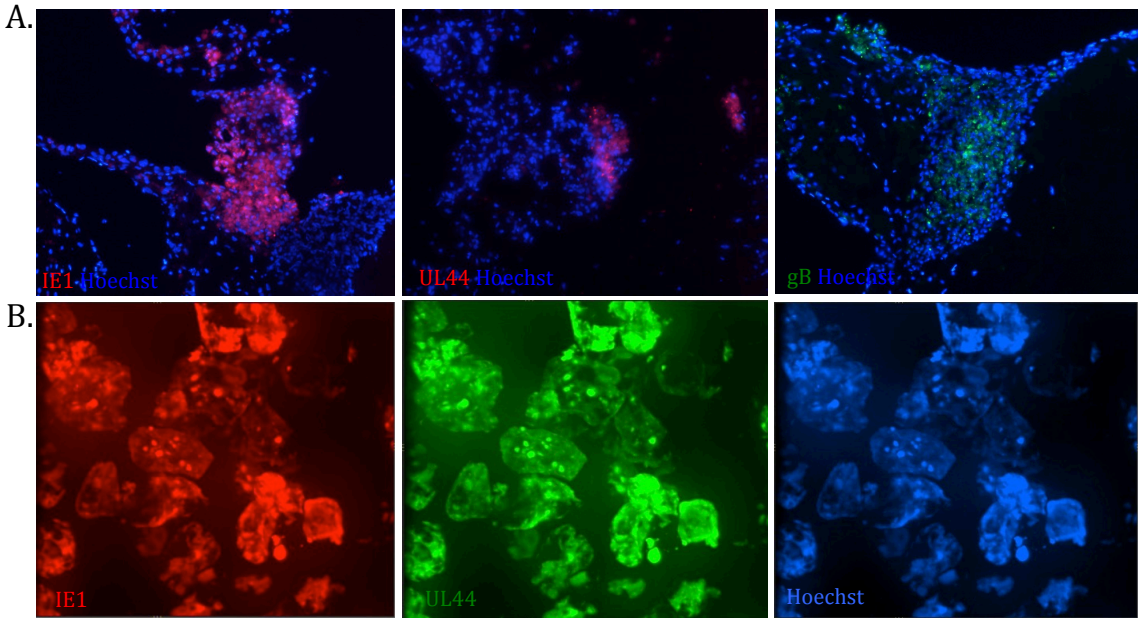

Figure 32: Cerebral organoids showed viral antigen positivity for different classes of viral proteins. (A) They stained positive for immediate early protein IE1 (left), early protein UL44 (middle), and late protein gB (right). (B) Confocal microscopy confirmed viral antigens were localized to the nucleus, as would be expected.

Beta tubulin III Localization in Infected Organoids

Preliminary data showed infected neurons derived from iPSCs (2D culture) had abnormal beta tubulin III staining patterns (Figure 9 in chapter one). Beta tubulin III is present in neuronal axons and the staining pattern normally shows long projections. In infected neurons, these projections were substantially shorter. Uninfected cells adjacent to infected cells also showed truncated projections. To compare the pattern of cellular protein expression between infected and uninfected organoids, we used immunofluorescence. Uninfected organoids show a similar staining pattern of beta tubulin III, with long axonal projections (Figure 33). In infected organoids, the areas of

viral antigen positivity had a complete absence of normal beta tubulin III projections (Figure 34). Directly adjacent to viral antigen positive regions there were normal staining patterns.

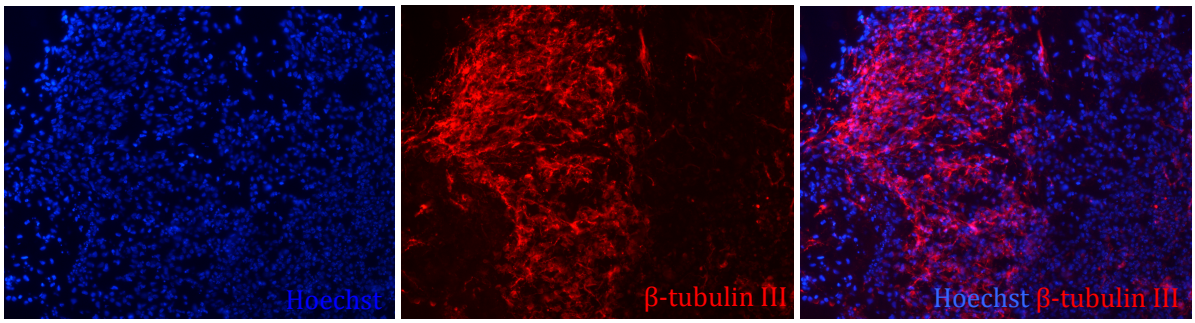

Figure 33:Uninfected cerebral organoids show a similar staining pattern of beta tubulin III to neurons derived from iPSCs, with long axonal projections.

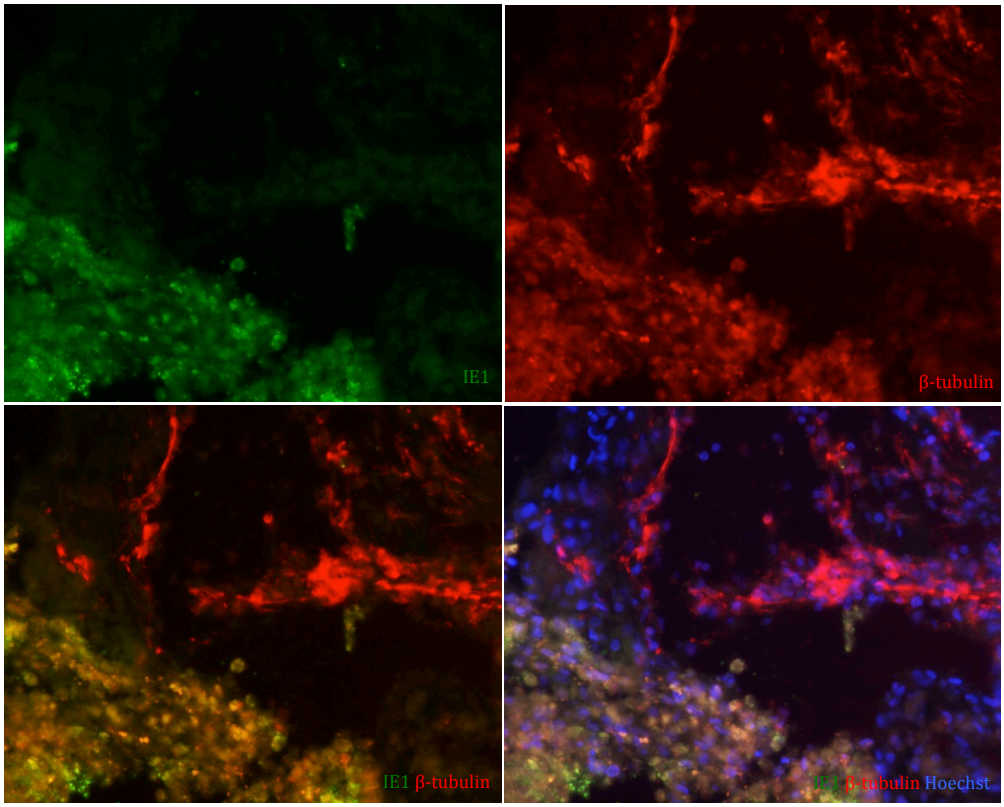

Figure 34: Beta tubulin III staining in the presence of viral antigen IE1. In areas of viral antigen positivity, there is an absence of normal beta tubulin III projections. Directly adjacent to viral antigen positive regions, there are normal staining patterns with long projections.

Nidogen-1 Localization in Mock and HCMV Infected Organoids

The extracellular matrix protein that lies upstream of the 1q42 break sites, nidogen-1, is present in cerebral organoids. Immunofluorescence showed nidogen-1 staining around the outer rim of cerebral structures, appearing to perform a supportive function for these structures. It also overlays the supportive structures mentioned above, further suggesting that these structures provide physical support for cerebral structures (Figure 35a). Epifluorescence appeared to show a dramatic decrease in nidogen-1 expression in areas of viral antigen positivity, parallel to transcription data (Figure 35b). Further confocal microscopy imaging showed that infected cells have a complete absence of nidogen-1 expression (Figure 34c).

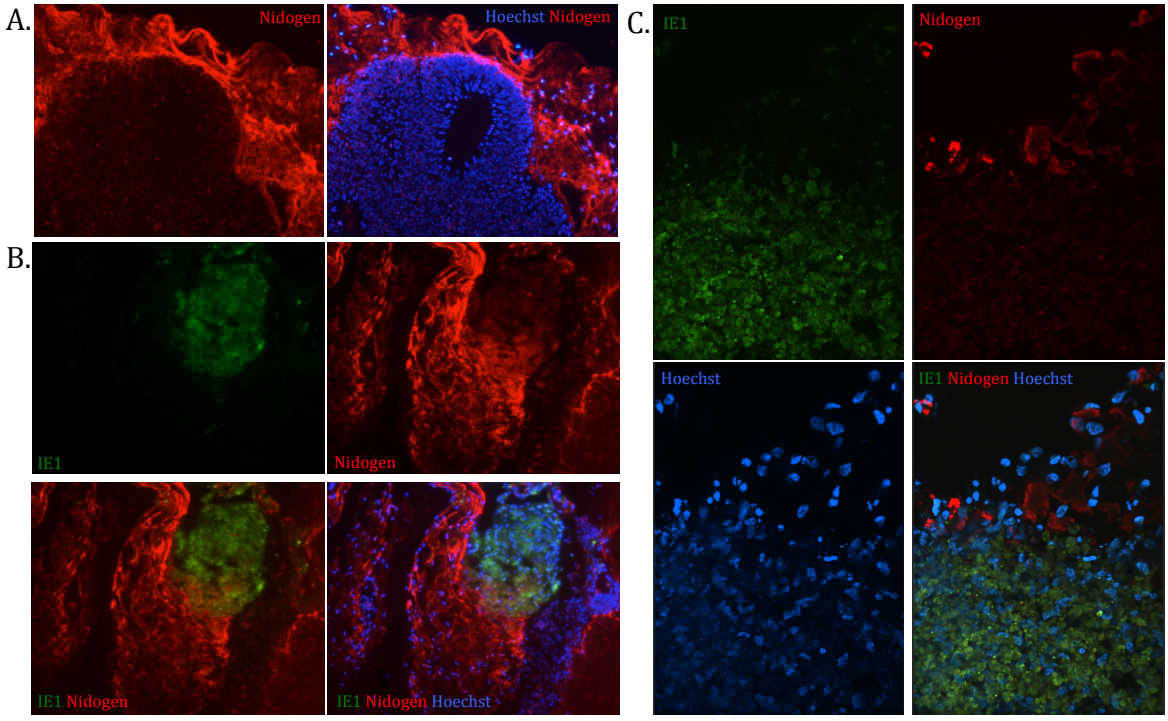

Figure 35: Localization of nidogen-1 staining in mock and HCMV-infected organoids. (A) Immunofluorescence staining showed nidogen-1 is localized around the outer rim of cerebral structures, appearing to perform a supportive function for these structures. (B) Nidogen-1 staining in the presence of viral antigen IE1. In areas of viral antigen positivity, there was a decreased expression of nidogen-1. (C) A single plane of a confocal image showed viral antigen IE1 staining in the nucleus and an absence of nidogen-1 staining in areas of viral antigen positivity.

Whole Organoid Imaging

Stereoscope images were taken of whole organoids derived with the new culling protocol in order to calculate approximate volumes. To explore the possibility of visualizing internal structures within a whole organoid, we used confocal microscopy to image through them. We utilized the auto-fluorescence of paraformaldehyde to try to observe the internal cerebral structures of the organoids. The resulting z stacks were projected to one plane, and then pieced together to form an image of the entire tissue. The confocal images were compared to stereoscope images of the same tissue (Figure

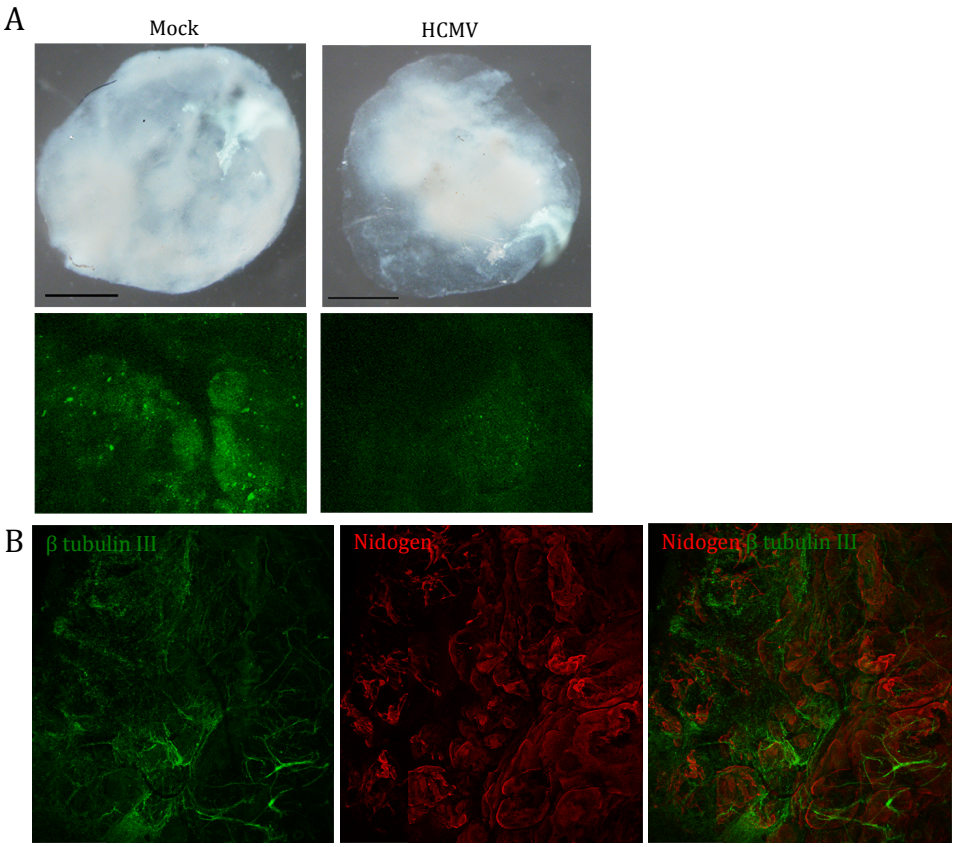

Figure 36: Whole organoid imaging of mock and HCMV infected whole organoids. (A) Stereoscope images (top) and autofluorescent (bottom) images were compared. Scale bar = 1 mm. (B) Confocal image of a randomly selected mock organoid stained for beta tubulin III and nidogen-1 using immunofluorescence. The staining patterns suggest the presence of internal cerebral structures.

36a). Based on the confocal images, we sorted put the organoids into categories based on the presence of possible cerebral structures. They were sorted into one of three categories: no structural definition, ill-defined structures, and multiple well defined structures. To determine if the confocal images and their corresponding structural category do indeed correlate to the presence of internal cerebral structures, the organoids will be sectioned.

One randomly selected mock whole organoid was stained with nidogen-1 and beta tubulin III using immunofluorescence to determine if what we saw on the autofluorescence images were indeed structures. This organoid stained strongly for both nidogen-1 and beta tubulin III and the staining pattern suggested the presence of internal cerebral structures (Figure 36b). One randomly selected infected whole organoid was stained with viral antigen IE1 and nidogen-1 to determine the spatial

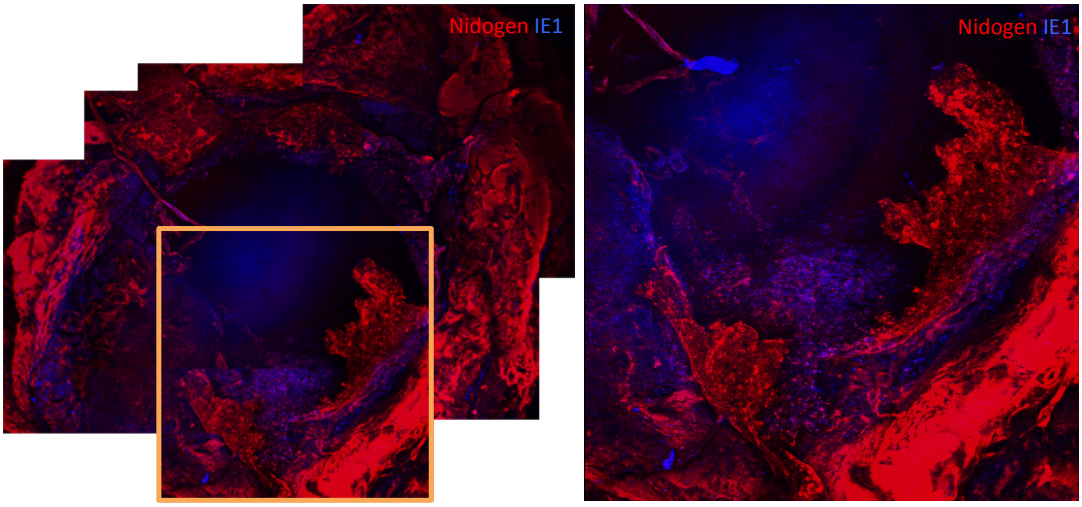

Figure 37: Stitched confocal image of a whole infected organoid stained for nidogen-1 and viral antigen IE1 (left). The orange box indicates the portion of the organoid that is magnified (right). Areas of viral antigen positivity show a decreased level of nidogen-1 compared to adjacent regions that are viral antigen negative

layout of viral antigen positive cells inside the whole organoid. This organoid showed decreased nidogen-1 expression in areas of viral antigen IE1 positivity (Figure 37).

Discussion and Conclusions

Cerebral organoids provide us a more clinically relevant model in which to study congenital HCMV infection than 2D culture of neurons or glia alone. They can mimic the internal architecture of the brain and can allow us to study infection at very early time points that can't be seen with clinical samples or 2D cell culture.

Our organoids are comparable to those previously described (Lancaster et al 2013) and have cerebral-like structures which resemble the SVZ of the developing brain and stain positive for the correct markers. The SVZ houses a population of NPCs and neural stem cells that migrate from the ventricular surface to the cortical plate as they differentiate into neurons. The interior of the cerebral structures stains positive for PAX6, which is an NPC marker. The outer and inner rim of the cerebral structures stains positive for beta-tubulin III, a neuron marker. This suggests that the innermost portion of the cerebral structures resembles the ventricular surface and the periphery of the structures resembles the cortical plate. As the NPCs differentiate into neurons, they migrate to the periphery of cerebral structures.

Our organoids also have supportive-like structures that appear to provide an extracellular matrix for the cerebral structures. Although supportive structures can be seen in previously described organoids, no attention is drawn to their existence. The

supportive structures also stain positive for 1q42 break site protein nidogen-1, which is a basement membrane protein that is developmentally important for the migration of neurons from the SVZ to the cortical plate. The presence of nidogen-1 around the periphery of the cerebral structures suggests that supportive structures resemble the pial membrane.

Fetuses that are infected during the first half of gestation develop more serious neurological defects than those infected later. We have modeled an early infection time by infecting iPSCs before organoid differentiation. We found that iPSCs are susceptible to HCMV infection before undergoing differentiation, but are not permissive. The cells become fully permissive 6 dpi, at which time they have begun the organoid differentiation process. Fully formed organoids express all three classes of viral antigens (IE, E, and L) in focal regions, suggesting they are supporting a full cycle of infection. Because microcephaly is a common neurological defect congenitally infected infants, we wanted to compare the overall size of mock and HCMV infected organoids. We calculated approximate volumes of both mock and infected organoids. Although there is no statistically significant difference between the two groups, we plan to investigate the size of the cerebral structures themselves.

Whole organoid confocal auto-fluorescence imaging appears to show internal cerebral structures. A randomly selected mock organoid stained for nidogen-1 and beta tubulin III showed patterns reminiscent of cerebral structures, but the organoids will need to

be sectioned to determine if the auto-fluorescent images correlate to actual cerebral structures.

Infected organoids have an abnormal beta tubulin III staining pattern, which is also seen in iPSC-derived neurons. Distinct beta tubulin III projections are absent in infected organoids and truncated in iPSC-derived neurons, suggesting impaired neuronal differentiation. Nidogen-1 is down regulated in viral antigen positive regions of infected organoids, as shown by epifluorescent imaging of organoid sections and confocal imaging of whole organoids. Confocal imaging of organoid sections showed a complete lack of nidogen-1 expression in HCMV infected cells. HCMV-induced down regulation of nidogen-1 could possibly hinder the migration of differentiating neurons, parallel to previous work in which mice with a mutation in the nidogen-1 binding site of laminin. In these mice, migrating neurons either prematurely ended their migration into the cortical plate or migrated past the meninges (Halfter et al. 2002)

CHAPTER FOUR: FUTURE DIRECTIONS

Future Directions

HCMV Induced Breaks on Chromosome One

Both chromosome one break sites are structurally similar with CTCF binding sites, DNAse hypersensitivity sites, and genes that are down regulated upon infection with HCMV. With this structural similarity, as well as a high degree of sequence homology to the HCMV genome, we think the breaks at both 1q42 and 1q23 are caused by a similar viral protein interaction. The next goal of this project is to map the DNA damage at 1q23 with LM-PCR. 1q42 and 1q23 are very similar, but there are a few important differences, which may pose some challenges. The 1q23 locus is highly repetitive and contains the same 7 kbp sequence repeated in tandem. A break could occur at any one of these repeats, or at all of them simultaneously. This region is also GC rich (~72%), which could cause difficulties with LM-PCR amplification.

The next goal of the project is to investigate how a viral protein (pp71) is interacting with the DNA or with cellular proteins (CTCF). To do this, we will determine if CTCF, pp71, or both are bound to the chromosome one break sites in mock and infected samples. Preliminary work using ChIP has shown that CTCF is bound at the 1q42 break site after infection with HCMV. Next, we will determine if pp71 is bound to the same site during infection and if pp71 and CTCF are directly interacting with one another.

Cerebral Organoids

Microcephaly is a common defect seen in infants who were congenitally infected with HCMV. These infants have a smaller brain and head than normal. Because of this, we expected infected cerebral organoids to have a smaller overall size relative to uninfected organoids. We found that there was no statistically significant difference in the estimated volume of infected and uninfected organoids. Although this surprised us, we plan to look at the size and organization of internal cerebral structures. Previously described cerebral organoids were used to study genetic microcephaly (Lancaster et al. 2013). They looked specifically at the mitotic spindle organization of radial glia and found that patient derived organoids had oblique and vertical oriented spindles, while normal organoids had exclusively horizontal spindles (Lancaster et al. 2013). They also found that patient derived organoids had a decreased pool of NPCs and more neurons, suggesting premature neuronal differentiation (Lancaster et al. 2013). We intend to investigate the presence of these features in infected organoids.

We have generated confocal images of whole organoids by projecting the entire z stack on to one plane. These images gave us a spatial layout of viral antigen, beta tubulin III, and nidogen-1 within the organoid. Projecting the whole organoid image on to one plane limits our ability to visualize the three dimensional internal structures of the organoid. Using these whole organoid confocal images, we want to create 3D reconstructions by stitching together each plane of the z stack individually.

Using cerebral organoids, we have modeled HCMV infection during early gestation in which the most severe birth defects occur. To study the consequences of later infection, we plan to infect organoids at different time points during differentiation. Previous research has shown that NPCs within the SVZ are preferentially infected by HCMV. This suggests that virus enters the developing brain through the ventricles, essentially placing contact directly in the interior. To mimic this infection route on more mature organoids, we will microinject HCMV into the interior. "Average" sized organoids will be harvested in order to count the number of cells and determine MOI.

In the present cerebral organoid experiments, we have used the iPSC line sc30i. When infected with HCMV, the virus is able to enter ~25-30% of sc30i cells. Another iPSC cell line, sc27i, is more susceptible to HCMV infection with entry occurring in ~50% of cells. We plan to repeat the previous studies investigating viral antigen, beta tubulin III, and nidogen-1 expression, as well as overall size and structure of organoids derived from sc27i cells.

From our initial experiments with cerebral organoids, we have shown a clear down regulation of nidogen-1 in viral antigen positive regions. The next step in these experiments is to culture cerebral organoids from nidogen-1 knockout cells. We are most interested to see if cerebral structures form in these organoids and if there is premature differentiation of neurons and proper localization of beta tubulin III.

We will use clinical cerebral samples to compare our findings in cerebral organoids. We will stain infected and uninfected clinical samples for nidogen-1 and look for similarities in staining pattern compared to organoids. Serial sections will be stained for viral antigens and nidogen-1 to determine if there is down regulation of nidogen-1 in infected regions.

The long-term goal of this project is to determine how pp71 interaction with the break sites is causing down regulation of both nidogen-1 and MPZ. The breaks could be interrupting an enhancer for these genes, or there could be epigenetic modifications of chromatin looping occurring at these sites after infection. We also want to know why pp71 is specifically causing damage at these sites on chromosome one. If pp71 is interacting with CTCF at these sites, what makes these loci "special?" There are CTCF binding regions throughout the genome, but breaks only occur at 1q23 and 1q42 during infection. Why is pp71 targeting these regions? Additionally, we are interested in investigating what part of pp71 is important for DNA damage. Perhaps this can help us understand why other herpesviruses don't cause DNA breaks or down regulation of these genes during infection.

REFERENCES

Amelio, Antonio L., Peterjon K. McAnany, and David C. Bloom. "A chromatin insulator-like element in the herpes simplex virus 1 latency-associated transcript region binds CCCTC-binding factor and displays enhancer-blocking and silencing activities." *Journal of Virology* 80.5 (2006): 2358-2368.

Belzile, J.P., T.J. Stark, G.W. Yeo, and D.H. Spector. "Human cytomegalovirus infection of human embryonic stem cell-derived primitive neural stem cells is restricted at several steps but leads to the persistence of viral DNA." *Journal of Virology* 88.8 (2014): 4021-4039.

Benirschke, Kurt and Peter Kaufmann. *Pathology of the Human Placenta.* New York: Springer, 2000.

Boppana, S.B., L.B. Rivera, K.B. Fowler, M. Mach, and W.J. Britt. "Intrauterine transmission of cytomegalovirus to infants of women with preconceptional immunity." *New England Journal of Medicine* 344 (2001): 1366-1371.

Britt, B. Maturation and egress. In: Arvin A, Campadelli-Fiume G, Mocarski E, et al., editors. Human Herpesviruses: Biology, Therapy, and Immunoprophylaxis. Cambridge: Cambridge University Press; 2007. Chapter 20.

Cannon, M.J. "Congenital cytomegalovirus (CMV) epidemiology and awareness." *Journal of Clinical Virology* 2009; 46 [Suppl 4]: S6-10.

Cannon, M.J., and K.F. Davis. "Washing our hands of the congenital cytomegalovirus disease epidemic." *BMC Public Health* 5 (2005): 70.

Chaillet, Carina Y. Howell, Mona Melhem, Sadayuki Inoue, Jerry R. Kuszak, Koen DeGeest, and Albert E. Chung. "Neurologic defects and selective disruption of basement membranes in mice lacking enactin-1/nidogen-1." *Laboratory Investigation* 82.12 (2002): 1617-1630.

Chang, W. L., A. F. Tarantal, S. S. Zhou, A. D. Borowsky, and P. A. Barry. "A recombinant rhesus cytomegalovirus expressing enhanced green fluorescent protein retains the wild-type phenotype and pathogenicity in fetal macaques." *Journal of Virology* 76 (2002)**:** 9493-9504

Cibulskis, Kristian, Michael S. Lawrence, Scott L. Carter, Andrey Sivachenko, David Jaffe, Carrie Sougnez, Stacey Gabriel, Matthew Meyerson, Eric S. Lander, and Gad Getz. "Sensitive detection of somatic point mutations in impure and heterogeneous cancer samples." *Nature Biotechnology* 31 (2013): 213-219.

Cugola, Fernanda R, Isabella R. Fernandes, Fabiele B. Russo, Beatriz C. Freitas, Joao L.M. Dias, Katia P. Guimaraes, Cecilia Benazzato, Nathalia Almeida, Graciela C. Pignatari, Sarah Romero, Carolina M. Polonio, Isabela Cunha, CarlaL. Freitas, Wesley N. Brandao, Cristiano Rossato, David G. Andrade, Daniele de P. Faria, Alexandre T. Garcez, Carlos A. Buchpigel, Carla T. Braconi, Erica Mendes, Amadou A. Sall, Paolo M. de A. Zanotto, Jean Pierre S. Peron, Alysson R. Muotri, and Patricia C.V. Beltrao-Braga. "The Brazilian Zika virus causes birth defects in experimental models." *Nature* (2016)

D'Aiuto, Leonard, Roberto Di Maio, Brianna Heath, Giorgio Raimondi, Jadranka Milosevic, Annie M. Watson, Mikhil Bamne, W. Tony Parks, Lei Yang, Bo Lin, Toshio Miki, Jocelyn Danielle Mich-Basso, Ravit Arav-Boger, Etienne Sibille,

Sarven Sabunciyan, Robert Yolken, and Vishwajit Nimakaonkar. "Human induced pluripotent stem cell derived models to investigate human cytomegalovirus infection in neural cells." *PLOS One* 7.11 (2012).

Dabro, Benjamin W., Vinit B. Mahajan, Lokesh Gakhar, Jessica M. Skeie, Elizabeth Campbell, Shu Wu, Xinyu Bing, Kathleen J. Millen, William B. Dobyns, John A. Kessler, Ali Jalali, James, Cremer, Aberto Segre, J. Robert Manak, Kimberly A. Aldinger, Satoshi Suzuki, Nagato Natsume, Maya Ono, Huynh Dai Hai, Le Thi Viet, Sara Loddo, Enza M. Valente, Laura Bernardini, Nitin Ghonge, Polly J. Ferguson, and Alexander G. Bassuk. "Mutations in Extracellular Matrix Genes NID1 and LAMC1 Cause Autosomal Dominant Dandy-Walker Malformation and Occipital Cephaloceles." *Human Mutation* 34.8 (2013): 1075-1079.

Dang, J., S.K. Tiwari, G. Lichinchi, Y. Qin, V.S. Patil, A.M. Eroshkin, and T.M. Rana. "Zika virus depletes neural progenitors in human cerebral organoids through activation of the innate immune receptor TLR3." *Cell Stem Cell* 19 (2006).

de Vries, L.S., H. Gunardi, P.G. Barth, L.A. Bok, M.A. Verboon-Maciolek, F. Groenendaal. "The spectrum of cranial ultrasound and magnetic resonance imaging abnormalities in congenital cytomegalovirus infection." *Neuropediatrics* 35.2 (2004): 113-119.

de Vries, L.S., M.A. Verboon-Maciolek, F.M. Cowan, F. Groenendaal. "The role of cranial ultrasound and magnetic resonance imaging in the diagnosis of infections of the central nervous system." *Early Hum Dev* 82.12 (2006): 819-825.

Dollard SC, Grosse SD, Ross DS. "New estimates of the prevalence of neurological and sensory sequelae and mortality associated with congenital cytomegalovirus infection." *Rev Med Virol* 17.5 (2007): 355-363.

Dollard, Sheila C., Stephanie A.S. Staras, Minal M. Amin, D. Scott Schmid, and Michael J. Cannon. "National prevalence estimates for cytomegalovirus IgM and IgG avidity and association between high IgM antibody titer and low IgG avidity." *Clinical and Vaccine Immunology* 18.11 (2011): 1895-1899.

Dong, Lijin, Y. Chen, M. Lewis, J.C. Hsieh, J. Reing, J.R. Chaillet, C.Y. Howell, M. Melhem, S. Inoue, J.R. Kuszak, K. Degeest, A.E. Chung. "Neurologic defects and selective disruption of basement membranes in mice lacking entactin-1/nidogen-1." *Lab Invest* 82.12 (2002): 1617-1630.

Fink, Kathleen R., Mahesh M. Thapa, Gisele E. Ishak, Sumit Pruthi. "Neuroimaging of pediatric central nervous system cytomegalovirus infection." *RadioGraphics* 30.7 (2010).

Fisher, S., O. Genbacev, E. Maidji, L. Pereira. "Human cytomegalovirus infection of the placental cytotrophoblasts in vitro and in utero: implications for transmission and pathogenesis." *Journal of Virology* 74.15 (2000): 6808-6820.

Fortunato, Elizabeth A., Marie L. Dell'Aquila, and Deborah H. Spector. "Specific Chromosome 1 Breaks Induced by Human Cytomegalovirus." *PNAS* 97.2 (2000): 853-858.

Gabrielli, L., M.P. Bonasoni, D. Santini, G. Piccirilli, A. Chiereghin, E. Petrisli, R. Dolcetti, B. Guerra, M. Piccioli, M. Lanari, M.P. Landini, T. Lazzarotto. "Congenital cytomegalovirus infection: patterns of fetal brain damage." *Clinical Microbiology and Infection* 18.10 (2012): 1049-1050.

Gabrielli, Liliana, Maria Paola Bonasoni, Donatella Santini, Giulia Piccirilli, Angela Chiereghin, Brunella Guerra, Maria Paola Landini, Maria Grazia Capretti, Marcello Lanari, and Tiziana Lazzarotto. "Human fetal inner ear infection involvement in congenital cytomegalovirus infection." *Acta Neuropathologica* 1.63 (2013).

Gage, F.H. "Mammalian neural stem cells." *Science* 287 (2000): 1433-1438.

Gross, Scott D., Danielle S. Ross, and Sheila C. Dollard. "Congenital cytomegalovirus (CMV) infection as a cause of permanent bilateral hearing loss: A quantitative assessment." *Journal of Clinical Virology* 41.2 (2007): 57-62.

Gude, N.M., C.T. Roberts, B. Kalionis, and R.G. King. "Growth and function of the normal human placenta." *Thromb Res* 114.5-6 (2004): 397-407.

Halfter, Willi, Sucai Dong, Yi-Ping Yip, Michael Willem, and Ulrike Mayer. "A critical function of the pial basement membrane in cortical histogenesis." *The Journal of Neuroscience* 22.14 (2002): 6029-6040.

Hardy, Kate, Alan H. Handyside, and Robert M.L. Winston. "The human blastocyst: cell number, death, and allocation during late perimplantation development in vitro." *Development* 107 (1989): 597-604.

Hayward, Jean C., David S. Titelbaum, Robert R. Clancy, and Robert A. Zimmerman. "Lissencephaly-Pachygyria associated with congenital cytomegalovirus infection." *Journal of Child Neurology* 6.2 (1991): 109-114.

Ishiyama Akira, Sarah E. Mowry, Ivan A. Lopez, and Gail Ishiyama. "Immunohistochemical distribution of basement membrane proteins in the human inner ear from older subjects." *Hearing Research* 254.1 (2009): 1–14.

Kalejta, Robert F. "Tegument proteins of human cytomegalovirus." *Microbiology and Molecular Biology Reviews* 72.2 (2008): 249-265.

Katano, Harutaka, Yuko Sato, Yoshihiro Tsutsui, Tetsutaro Sata, Akihiko Maeda, Naoki Nozawa, Naoki Inoue, Yasuya Nomura, Takeshi Kurata. "Pathogenesis of cytomegalovirus-associated labrynthitis in a guinea pig model." *Microbes and Infection* 9 (2007): 183-191.

Kawasaki, H., I. Kosugi, Y. Arai, and Y. Tsutsui. "The amount of immature glial cells in organotypic brain slices determines the susceptibility to murine cytomegalovirus infection." *Laboratory Investigation* 82 (2002): 1347-1358.

Koboldt, D.C., Q. Zhang, D.E. Larson, D. Shen, M.D. McLellan, L. Lin, C.A. Miller, E.R. Mardis, L. Ding, R.L. Wilson. "VarScan 2: Somatic mutation and copy number alteration discovery in cancer by exome sequencing." *Genome Research* 22.3 (2012): 568-576.

Kong, Qingzhong and Nancy Maizels. "Breaksite batch mapping, a rapid method for assay and identification of DNA breaksites in mammalian cells." *Nucleic Acids Reserch* 29.6 (2001).

Kosugi, I., H. Kawasaki, Y. Arai, and Y. Tsutsui. "Innate immune responses to cytomegalovirus infection in the developing mouse brain and their evasion by virus-infected neurons." *Am. J. Pathol.* 161 (2002): 919-928.

Lancaster, Madeline A. and Juergen A. Knoblich. "Generation of cerebral organoids from human pluripotent stem cells." *Nature Protocols* 9.10 (2014): 2329-2340.

Lancaster, Madeline A., Magdalena Renner, Carol-Anne Martin, Daniel Wenzel, Louise S. Bicknell, Matthew E. Hurles, Tessa Homfray, Josef M. Penninger, Andrew P.

Jackson, and Juergen A. Knoblich. "Cerebral organoids model human brain development and microcephaly." *Nature* 501.7467 (2013): 373-79.

Lee, Hyun Kyoung, In Ae Seo, Duk Joon Suh, and Hwan Tae Park. "Nidogen plays a role in the regenerative axon growth of adult sensory neurons through Schwann cells." *Journal of Korean Medical Science* 24.4 (2009): 654-659.

Lee, Hyun Kyoung, In Ae Seo, Hye Kyung Park, Yoo Mi Park, Kyoung Jin Ahn, Young, Hyun Yoo, and Hwan Tae Park. "Nidogen is a prosurvival and promigratory factor for adult Schwann cells." *Journal of Neurochemistry* 102.3 (2007): 686-698.

Li, R.Y. and Y. Tsutsui. "Growth retardation and microcephaly induced in mice by placental infection with murine cytomegalovirus." *Teratology* 62 (2000): 29-85.

Lokensgard, J.R., M.C. Cheeran, G. Gekker, S. Hu, C.C. Chao, P.K. Peterson. "Human cytomegalovirus replication and modulation of apoptosis in astrocytes." *J Hum Virol* 2.2 (1999): 91-101.

Lukashchuk, V., S. McFarlane, R.D. Everett, and C.M. Preston. "Human cytomegalovirus protein 9971 displaces the chromatin-associated factor ATRX from nuclear domain 10 at early stages of infection." *Journal of Virology* 82 (2008): 12543-12554.

Luo, Min Hua, Holger Hannemann, Amit S. Kulkarni, Philip H. Schwartz, John M. O'Dowd, and Elizabeth A. Fortunato. "Human Cytomegalovirus Infection Causes Premature and Abnormal Differentiation of Human Neural Progenitor Cells." *Journal of Virology* 84.7 (2010): 3528-541.

Luo, Min Hua, Philip H. Schwartz, and Elizabeth A. Fortunato. "Neonatal Neural Progenitor Cells and Their Neuronal and Glial Cell Derivatives Are Fully Permissive for Human Cytomegalovirus Infection." *Journal of Virology* 82.20 (2008): 9994-10007.

Maidji, Ekaterina, Elena Percivalle, Guiseppe Gerna, Susan Fisher, and Lenore Pereira. "Transmission of human cytomegalovirus from infected microvascular endothelial cells to differentiating/invasive placental cytotrophoblasts." *Virology* 304.1 (2002): 53-69.

Martinez, F.P., R. Cruz, F. Lu, R. Plasschaert, Z. Deng, Y.A. Rivera-Molina, M.S. Bartolomei, P.M. Lieberman, Q. Tang. "CTCF binding to the first intron of the major immediate early gene of human cytomegalovirus (HCMV) negatively regulates MIE gene expression and HCMV replication." *Journal of Virology* 88.13 (2014): 7389-7401.

Mayhew, T.M., C. Ohadike, P.N. Baker, I.P. Crocker, C. Mitchell, S.S. Ong. "Stereological investigation of placental morphology in pregnancies complicated by pre-eclampsia with and without intrauterine growth restriction." *Placenta* 24.2-3 (2003): 219-226.

Melnick, Michael and Tina Jaskoll. "An in vitro mouse model of congenital cytomegalovirus-induced pathogenesis of the inner ear cochlea." *Birth Defects Res A Clin Mol Teratol* 97.2 (2013): 69-78.

Mutnal, Manohar B., Maxim C-J. Cheeran, Shuxian Hu, and James R. Lokensgard. "Murine cytomegalovirus infection of neural stem cells alters neurogenesis in the developing brain." *PLOS One* 6.1 (2011): e16211.

Najm, J., D. Horn, I Wimplinger, J.A. Golden, V.V. Chizhikov, J. Sudi, S.L. Christian, R. Ullmann, A. Kuechler, C.A. Haas, A. Flubacher, L.R. Charnas, G. Uyanik, U. Frank, E. Klopocki, W.B. Dobyns, K. Kutsche. "Mutations of CASK cause an X-linked brain malformation phenotype with microcephaly and hypoplasia of the brainstem and cerebellum." *Nature Genetics* 40.9 (2008): 1065-1067.

Nakamura, Hiroyuki, Huanan Liao, Kahori Minami, Masashi Toyoda, Hidenori Akitsu, Yoshitaka Miyagawa, Hajime Okita, Nokutaka Kiyokawa, Akihiro Imezawa, Ken-Ichi Imadome, Naoki Inoue, and Shigeyohsi Fujiwara. "Human cytomegalovirus induces apoptosis in neural stem/progenitor cells derived from induced pluripotent stem cells by generating mitochondrial dysfunction and endoplasmic reticulum stress." *Herpesviridae* 4.1 (2013).

Nelson, C.T. and G.J. Demmler. "Cytomegalovirus infection in the pregnant mother, fetus, and newborn infant." *Clin. Perinatol.* 24 (1997):151-160.

Noyola, D.E., G.J. Demmler, C.T. Nelson, C. Griesser, W.D. Williamson, J.T. Atkins, J. Rozelle, M. Turcich, A.M. Llorente, S. Sellers-Vinson, A. Reynolds, J.F. Bale Jr., P. Gerson, and M.D. Yow. "Early predictors of neurodevelopmental outcome in symptomatic congenital cytomegalovirus infection." *Journal of Pediatrics* 138.3 (2001): 325-331.

O'Dowd, John M., Anamaria G. Zavala, Celeste J. Brown, Toshio Mori, and Elizabeth A. Fortunato. "HCMV-infected cells maintain efficient nucleotide excision repair of the viral genome while abrogating repair of the host genome." *PLOS Pathogens* 8.11 (2012).

Ong, Chin-Tong and Victor G. Corces. "CTCF: An architectural protein bridging genome topology and function." *Nature Reviews Genetics* 15 (2014): 234-246.

Pass, R.F., K.B. Fowler, S.B. Boppana, W.J. Britt, S. Stagno. "Congenital cytomegalovirus infection following first trimester maternal infection: symptoms at birth and outcome." *Journal of Clinical Neurology* 35.2 (2005): 216-220.

Penkert, Rhiannon R. and Robert F. Kalejta. "Human embryonic stem cell lines model experimental human cytomegalovirus latency." *MBio* 4.3 (2013).

Poland, Stephen D., Penny Costello, Gregory A. Dekaban and G.P.A Rice. "Cytomegalovirus in the brain: In vitro infection of human brain-derived cells." *The Journal of Infectious Diseases* 162.6 (1990): 1252-1262.

Pulliam, Lynn, Dan Moore, and David C. West. "Human cytomegalovirus induces IL-6 and TNFα from macrophages and microglia cells: Possible role in neurotoxicity." *Journal of Neurovirology* 1.2 (1995): 219-227.

Reuter, Jon D., Daniel L. Gomez, Jean H. Wilson, and Anthony N. Van den Pol. "Systemic immune deficiency necessary for cytomegalovirus invasion of the mature brain." *Journal of Virology* 78.3 (2004): 1473-1487.

Ryckman, Brent J., Barb L. Rainish, Marie C. Chase, Jamie A. Borton, Jay A. Nelson, Michael A. Jarvis, and David C. Johnson. "Characterization of the human cytomegalovirus gH/gL/UL128-131 complex that mediates entry into epithelial and endothelial cells." *Journal of Virology* 82.1 (2007): 60-70.

Schleiss, Mark R. and Michael McVoy. "Guinea pig cytomegalovirus (GPCMV): A model for the study of the prevention and treatment of maternal-fetal transmission." *Future Virology* 5.2 (2010): 207-217.

Shinmura, Y., I. Kosugi, S. Aiba-Masago, S. Baba, L.R. Yong, and Y. Tsutsui. "Disordered migration and loss of virus-infected neuronal cells in developing mouse brains infected with murine cytomegalovirus." *Acta Neuropathologica* 93.6 (1997): 551-557.

Sinclair, John and Patrick Sissons. "Latency and reactivation of human cytomegalovirus." *Journal of General Virology* 87 (2006): 1763-1779.

Staras, S. A., S. C. Dollard, K. W. Radford, W. D. Flanders, R. F. Pass, and M. J. Cannon. 2006. "Seroprevalence of cytomegalovirus infection in the United States, 1988–1994." *Clinical Infectious Diseases* 43 (2006):1143–1151.

Su, Ying, David G. Brooks, Yanling Li, Jacques Lebercq, James A. Trofatter, Jeffrey V. Ravetch, and Roger V. Lebo. "Myelin protein zero gene mutated in Charcot-Marie-Tooth type 1B patients." *PNAS* 90.22 (1993): 10856-10860.

Tabata, Takako, Matthew Petitt, June Fang-Hoover, Jose Rivera, Naoki Nozawa, Stephen Shiboski, Naoki Inoue, and Lenore Pereira. "Cytomegalovirus impairs cytotrophoblast-induced lymphangiogenesis and vascular remodeling in an *in vivo* human placentation model." *The American Journal of Pathology* 181.5 (2012): 1540-1559.

Tabata, Takako, Matthew Petitt, Martin Zydek, June Fang-Hoover, Nicholas Larcocque, Mitsuru Tsuge, Matthew Gormley, Lawrence M. Kauvar, and Lenore Pereira. "Human cytomegalovirus infection interferes with the maintenance and differentiation of trophoblast progenitor cells of the human placenta." *Journal of Virology* 89.9 (2015): 5134-5147.

Takahashi, Kazutoshi and Shinya Yamanaka. "Induction of pluripotent stem cells from mouse embryonic and adult fibroblast cultures by defined factors." *Cell* 126.4 (2006): 663-676.

Tamashiro, J.C., L.J. Hock, and D.H. Spector. "Construction of a cloned library of the EcoRI fragments from the human cytomegalovirus genome (strain AD169) *Journal of Virology* 2.2 (1982): 547-557.

Teissier, Natacha, Anne-Lise Delezoide, Anne-Elisabeth Mas, Suonavy Khung-Savatovsky, Bettina Bessieres, Jeannette Nardelli, Christelle Vauloup-Fellous, Olivier Picone, Nadira Houhou, Jean-Francois Oury, Thierry Van Den Abbeele, Pierre Gressens, Homa Adle-Biassette. "Inner ear lesions in congenital cytomegalovirus infection of human fetuses." *Acta Neuropahologica* 122.6 (2011): 763-774.

Teissier, Natacha, Catherine Fallet-Bianco, Anne-Lise Delezoide, Annie Laquerriere, Pascale Marcorelles, Suonavy Khung-Savatovsky, Jeanette Nardelli, Sara Cipriani, Zsolt Csaba, Oliver Picone, Jeffrey A. Golden, Thierry Van Den Abbeele, Pierre Gressens, and Homa Adle-Biassette. "Cytomegalovirus-induced brain malformations in fetuses." *Journal of Neuropathology and Experimental Neurology* 73.2 (2014): 143-158.

Tomtishen III, John Paul. "Human cytomegalovirus tegument proteins (pp65, pp71, pp150, pp28)." *Virology Journal* 9.22 (2012).

van der Knaap, MS, G. Vermeulen, F. Barkhof, A.A. Hart, J.G. Loeber, and J.F. Weel. "Pattern of white matter abnormalities at MR imaging: use of polymerase chain reaction testing of Guthrie cards to link pattern with congenital cytomegalovirus infection." *Radiology* 230.2 (2004): 529-536.

Varnum, S.M., D.N. Streblow, M.E. Monroe, P. Smith, K.J. Auberry, L. Pasa-Tolic, D. Wang, D.G. Camp II, K. Rodland, S. Wiley, W. Britt, T. Shenk, R.D. Smith, and J.A. Nelson. "Identification of proteins in human cytomegalovirus (HCMV) particles: The HCMV proteome." *Journal of Virology* 78.20 (2004): 10960-10966.

Vasudevan, A., M.S. Ho, M. Weiergraber, R. Nischt, T. Schneider, A. Lie, N. Smyth, and R. Kohling. "Basement membrane protein nidogen-1 shapes hippocampal synaptic plasticity and excitability." *Hippocampus* 20.5 (2010) 608-620.

Wang, Jue, Baofu Zhang, Hui Jiang, Lei Zhang, Danzheng Liu, Xiao Xiao, Hanna Ma, Xuemei Luo, Dennis Bojrab II, and Zhengqing Hu. "Myelinatioin of the postnatal mouse cochlear nerve at the peripheral-central nervous system transition zone." *Frontiers in Pediatrics* 43.1 (2013).

Woodhall, D.L., I.J. Groves, M.B. Reeves, G. Wilkinson, J.H. Sinclair. "Human Daxx-mediated repression of human cytomegalovirus gene expression correlates with a repressive chromatin structure around the major immediate early promoter." *J. Biol. Chem.* 281 (2008): 37652-37660.

Zhou, M., J.M. Lanchy, and B.J. Ryckman. "Human cytomegalovirus gH/gL/gO promotes the fusion step of entry into all cell types, whereas gH/gH/UL128-131 broadens virus tropism through a distinct mechanism." *Journal of Virology* 89.17 (2015).

Zhou, M., Q. Yu, A. Wechsler, B.J. Ryckman. "Comparative analysis of gO isoforms reveals that strains of human cytomegalovirus differ in the ratio of gH/gL/gO and gH/gL/UL128-131 in the virion envelope." *Journal of Virology* 87.17 (2013): 9680-9690.

Zhou, Y., S.J. Fisher, M. Janatpour, O. Genbacev, E. Dejana, M. Wheelock, and C.H. Damsky. "Human cytotrophoblasts adopt a vascular phenotype as they differentiate. A strategy for successful endovascular invasion?" *J Clin Invest* 99.9 (1997): 2139-2151.

Zucca, C., S. Binda, R. Borgatti, F. Triulzi, L. Radice, C Butte, P.E. Barkhaus, and M. Barbi. "Retrospective diagnosis of congenital cytomegalovirus infection and cortical maldevelopment." *Neurology* 61.5 (2003): 710-712.

APPENDIX: PERMISSIONS

NATURE PUBLISHING GROUP LICENSE
TERMS AND CONDITIONS

May 24, 2016

This is a License Agreement between Rebecca M Brown ("You") and Nature Publishing Group ("Nature Publishing Group") provided by Copyright Clearance Center ("CCC"). The license consists of your order details, the terms and conditions provided by Nature Publishing Group, and the payment terms and conditions.

All payments must be made in full to CCC. For payment instructions, please see information listed at the bottom of this form.

License Number	3875620354834
License date	May 24, 2016
Licensed content publisher	Nature Publishing Group
Licensed content publication	Nature
Licensed content title	Cerebral organoids model human brain development and microcephaly
Licensed content author	Madeline A. Lancaster, Magdalena Renner, Carol-Anne Martin, Daniel Wenzel, Louise S. Bicknell et al.
Licensed content date	Aug 28, 2013
Volume number	501
Issue number	7467
Type of Use	reuse in a dissertation / thesis
Requestor type	academic/educational
Format	print and electronic
Portion	figures/tables/illustrations
Number of figures/tables/illustrations	2
High-res required	no
Figures	Figure 1a and Figure 3a.
Author of this NPG article	no
Your reference number	None
Title of your thesis / dissertation	Using Cerebral Organoids to Model HCMV Infection in the Developing Brain
Expected completion date	Jun 2016
Estimated size (number of pages)	100
Total	0.00 USD
Terms and Conditions	

Terms and Conditions for Permissions

Nature Publishing Group hereby grants you a non-exclusive license to reproduce this

NATURE PUBLISHING GROUP LICENSE
TERMS AND CONDITIONS

May 26, 2016

This is a License Agreement between Rebecca M Brown ("You") and Nature Publishing Group ("Nature Publishing Group") provided by Copyright Clearance Center ("CCC"). The license consists of your order details, the terms and conditions provided by Nature Publishing Group, and the payment terms and conditions.

All payments must be made in full to CCC. For payment instructions, please see information listed at the bottom of this form.

License Number	3876660672043
License date	May 26, 2016
Licensed content publisher	Nature Publishing Group
Licensed content publication	Nature Genetics
Licensed content title	Mutations of CASK cause an X-linked brain malformation phenotype with microcephaly and hypoplasia of the brainstem and cerebellum
Licensed content author	Juliane Najm, Denise Horn, Isabella Wimplinger, Jeffrey A Golden, Victor V Chizhikov et al.
Licensed content date	Aug 10, 2008
Volume number	40
Issue number	9
Type of Use	reuse in a dissertation / thesis
Requestor type	academic/educational
Format	print and electronic
Portion	figures/tables/illustrations
Number of figures/tables/illustrations	1
High-res required	no
Figures	Figure 2a and 2b
Author of this NPG article	no
Your reference number	None
Title of your thesis / dissertation	Using Cerebral Organoids to Model HCMV Infection in the Developing Brain
Expected completion date	Jun 2016
Estimated size (number of pages)	100
Total	0.00 USD
Terms and Conditions	

Terms and Conditions for Permissions

Nature Publishing Group hereby grants you a non-exclusive license to reproduce this